Complex Formation of ICL670 and Related Ligands with Fe^{III} and Fe^{II}

Stefan Steinhauser,[a] Uwe Heinz,[a] Mark Bartholomä,[a] Thomas Weyhermüller,[b] Hanspeter Nick,[c] and Kaspar Hegetschweiler*[a]

Keywords: Iron / Ligand design / Chelates / N,O ligands / Redox chemistry

Complex formation of 4-[3,5-bis(2-hydroxyphenyl)-1,2,4-triazol-1-yl]benzoic acid (ICL670, H_3L^x), 4-[3,5-bis(2-hydroxyphenyl)-1,2,4-triazol-1-yl]benzosulfonic acid (H_3L^y), and 3,5-bis(2-hydroxyphenyl)-1-phenyl-1,2,4-triazole (H_2L^z) with Fe^{3+} and Fe^{2+} was investigated in H_2O and in H_2O/DMSO mixtures by potentiometry, spectrophotometry and cyclic voltammetry. ICL670 has previously been considered as a promising drug for an oral treatment of iron overload. In this paper, the stability and redox properties of the various Fe^{II} and Fe^{III} complexes were elucidated with a particular focus on their potential involvement in the generation of oxidative stress. The overall stability constants of $[Fe^{III}(L^x)]$ and $[Fe^{III}(L^x)_2]^{3-}$ (25 °C, 0.1 M KCl in H_2O) are log β_1 = 22.0 and log β_2 = 36.9, respectively. The affinity of these ligands for Fe^{2+} is remarkably poor. In particular, the 1:2 complexes $[Fe^{II}(L^x)_2]^{4-}$ and $[Fe^{II}(L^y)_2]^{4-}$ were found to be less stable. As a consequence, the redox chemistry of the $[Fe^{III}(L^x)]/[Fe^{II}(L^x)]^-$ and the $[Fe^{III}(L^x)_2]^{3-}/[Fe^{II}(L^x)_2]^{4-}$ couples differs significantly. $[Fe^{III}(L^x)_2]^{3-}$ is a very weak oxidizing agent ($E_{1/2}$ is approximately –0.6 V versus NHE) and reduction of $[Fe^{III}(L^x)_2]^{3-}$ is not anticipated under physiological conditions. The reduction potential of the $[Fe^{III}(L^x)]/[Fe^{II}(L^x)]^-$ couple is considerably less negative and was estimated to be +0.1 V (versus NHE). The possible roles of the various Fe complexes as catalysts for the Fenton reaction in biological media are discussed. The crystal structures of H_3L^x, $Na[Fe(L^z)_2]\cdot 4EtOH$, $Na[Al(L^z)_2]\cdot 4EtOH$, and $[Cu(L^z)(pyridine)]_2$ were investigated by single-crystal X-ray diffraction, and the possible influence of the particular steric requirements of these ligands on the stability of the metal complexes has been analyzed.

1. Introduction

Iron, an essential bioelement, is toxic when present in excess.[1] Iron overload is a particularly grave condition, because the human body lacks a physiological mechanism for actively excreting iron. There are a variety of different causes for the excessive loading of iron in a person; an important one is regular blood transfusions, necessary in the treatment of hematological defects such as β-Thalassaemia. Consequently, transfusion therapy must be combined with the administration of an iron-binding agent, transforming excess body iron into a chelated, excretable form. Presently, the microbial siderophore desferrioxamine (desferal, DFO) is used for this purpose (Scheme 1). This ligand, however, has some drawbacks. DFO is orally inactive and has a rather short plasma half-life. The need for new orally active iron chelators has been recognized for more than 30 years.[2] Deferiprone (L1), a hydroxy-pyridinone, can be taken orally; however, its application does suffer from some side effects.[3] The compound 4-[3,5-bis(2-hydroxyphenyl)-1,2,4-triazol-1-yl]benzoic acid (ICL670, deferasirox) is also an orally active iron chelator.[4] In previous animal studies, it proved to be more effective than parenteral DFO,[5] ICL670 is presently in Phase III of clinical trials.

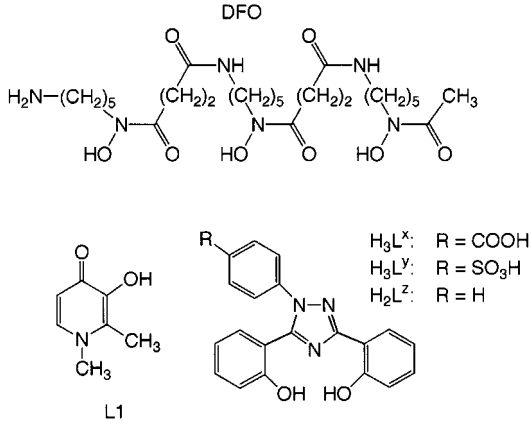

Scheme 1

A potential problem associated with iron chelation is the generation of oxidative stress.[6] Reactive oxygen species (ROS), and in particular the $OH^{\cdot}$ radical, have a consider-

[a] Anorganische Chemie, Universität des Saarlandes, Postfach 15 11 50, 66041 Saarbrücken, Germany
Fax: +49-681-302-2663
E-mail: hegetschweiler@mx.uni-saarland.de
[b] Max-Planck-Institut für Bioanorganische Chemie, Postfach 10 13 65, 45413 Mülheim an der Ruhr, Germany
[c] Novartis Institutes for BioMedical Research, WKL-136.P.72, Klybeckstrasse 141, 4002 Basel, Switzerland
Supporting information for this article is available on the WWW under http://www.eurjic.org or from the author.

able potential to damage a variety of cellular components.[7] There has been – and still is – a debate on the precise mechanism of oxidative stress.[8–11] It has been proposed that $OH^{\cdot}$ is generated by an Fe-catalyzed process; Fe^{III} is reduced by $O_2^{\cdot-}$ to Fe^{II}, which in turn reduces H_2O_2 to $OH^{\cdot}$ and OH^-.[7] It has also been argued that the level of O_2 in the cell would be much higher than that of H_2O_2, and that the initial step of oxidative stress could be assigned to the reaction of Fe^{II} with O_2 rather than H_2O_2.[12] Moreover, the reduction of Fe^{III} to Fe^{II} is not necessarily mediated by $O_2^{\cdot-}$, but could occur through the use of abundant biological reducing agents such as ascorbate and thiols.[7]

Although the precise mechanism of oxidative stress is not completely understood, it is generally accepted that iron can catalyze the production of ROS in terms of redox cycling, when it is available in a labile, redox-active form.[6–9,13–15] It is noteworthy that either a very high or a very low redox potential of an iron complex prevents oxidative stress. Ligands such as desferrioxamine or 1,10-phenanthroline, having either a high preference for the ferric or the ferrous form, appear to be inactive in terms of oxygen toxicity, whereas aminopolycarboxylates such as NTA^{3-}, $EDTA^{4-}$ or $DTPA^{5-}$ efficiently catalyze the production of single and double strand breaks of DNA and of modified nucleobases.[14] The reduction potential of possible $Fe^{III}L_n$/$Fe^{II}L_m$ species is thus a crucial parameter when developing new iron chelators for therapeutic use (Figure 1).[16]

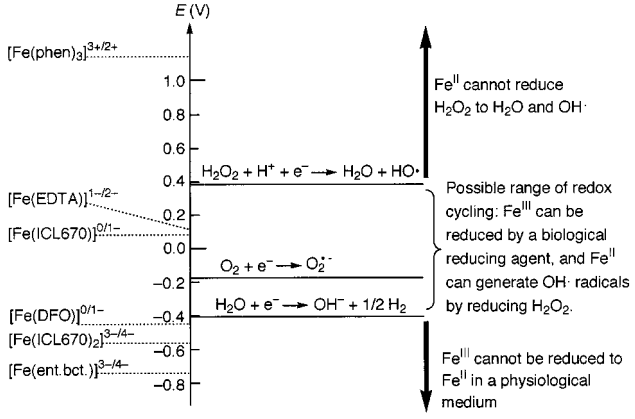

Figure 1. The possibility for redox cycling induced by different Fe^{III}/Fe^{II} complexes in biological media according to ref.[16]; the redox potentials are listed for pH 7, they were taken from refs.[16,18] and from this work (Fe–ICL670); the $O_2/O_2^{\cdot-}$ potential of −0.16 V refers to equal concentrations of dissolved O_2 and $O_2^{\cdot-}$, and not to the standard state (1 M $O_2^{\cdot-}$, 1 atm O_2); DFO = desferrioxamine, ent.bct = enterobactine, phen = 1,10-phenanthroline

In the present investigation, we address the problem of the possible redox activity of Fe–ICL670 complexes. For this purpose, we have studied the various species that form in solution, using a variety of physicochemical methods. Some preliminary results have already been published.[17] Herein, we present a comprehensive report on the complex formation of ICL670 (H_3L^x) and the related ligands H_3L^y and H_2L^z (Scheme 1) with Fe^{II} and Fe^{III}.[19–21]

2. Results

2.1. Solid-State Structures

2.1.1. Free Ligands

The unsubstituted derivative H_2L^z was first described by Ryabukhin.[21] We recently reported its crystal structure and documented the importance of the O–H···N hydrogen-bonding interactions between the phenolic hydroxy groups and N1 or N3 of the triazole ring.[22] Both O–H groups of H_2L^z are involved in intramolecular hydrogen bonds forming six-membered ring structures. O–H···N hydrogen bonding was also observed in the carboxylic acid derivative H_3L^x (ICL670), but in this ligand, only one of the hydroxy groups formed an intramolecular hydrogen bond (Figure 2). The other O–H···N bond was intermolecular, leading to infinite zigzag chains parallel to the crystallographic *z*-axis. These chains, which are further stabilized by some stacking interactions, are interconnected by the well-known pairing of the carboxylic acid moieties. The resulting two-dimensional sheets are oriented parallel to the *y*-*z* plane. Only one of the phenolic rings is roughly coplanar with the central triazole ring (the torsional angle is 2.3 °), while the other

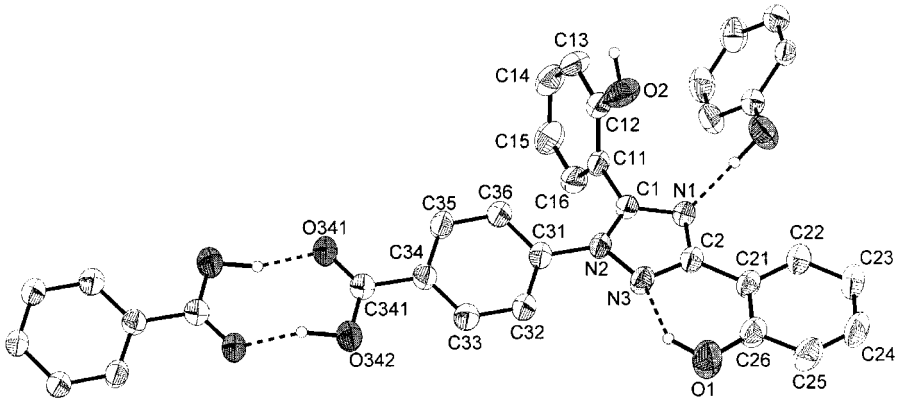

Figure 2. Molecular structure of H_3L^x (ICL670); the benzoic acid moiety and one phenol moiety of two neighboring H_3L^x molecules are also shown in order to illustrate the various types of intra- and intermolecular hydrogen bonding; atomic displacement ellipsoids are drawn at the 30% probability level; H(–O) hydrogen atoms are shown as spheres of arbitrary size; H(–C) hydrogen atoms are omitted for clarity. Bond lengths and angles are as expected

phenolic ring with a torsional angle of 77.7° stands almost perpendicular to the triazole moiety. The benzoic acid moiety is tilted slightly out of the triazole plane by an angle of 13.9°.

2.1.2. Metal Complexes

There have been several unsuccessful attempts to crystallize metal complexes with H_3L^x and H_3L^y. However, complex formation with H_2L^z yielded, a variety of crystalline materials. Single crystals of $Na[Fe(L^z)_2]\cdot 4EtOH$ were found to be very fragile and disintegrated rapidly in air (loss of EtOH). Moreover, the crystal structure of this complex proved to be severely disordered. Refinement of a data set collected at room temperature resulted in rather poor agreement factors.[23] This disorder could partially be resolved in a low-temperature experiment (100 K). Two superimposed conformers in a 2:1 ratio were located (Figure 3), and some constraints had to be used to model the C−C distances in the peripheral phenyl ring realistically. The $[Fe(L^z)_2]^-$ anion was located on a crystallographic C_2 axis. This resulted in additional disorder of the sodium counterion, which was found in proximity of this axis (the disorder remained when the data was refined in the lower-symmetry space group *C*/*c*). The structure of $Na[Al(L^z)_2]\cdot 4EtOH$ is isotypic, showing the same type of disorder as observed for the Fe complex.[24]

$[Fe(L^z)_2]^-$ adopts the expected bis-structure with a meridional coordination mode of the two L^z entities, a distorted octahedral coordination environment, and Fe−O distances at the short end of the range expected for high-spin Fe^{III}.[25] The Fe−N distance of 2.092(5) Å is also remarkably short. It is worth noting that the ligand in this complex is once again not planar. The torsional angles between the phenolate rings and the central triazole unit are 14.1° and 23.5° (for the isostructural $[Al(L^z)_2]^-$, the corresponding values are 14.0° and 19.6°).[24] The sodium counterion is associated with one phenoxo group of each ligand. Four EtOH moieties complete the roughly octahedral NaO_6 coordination environment.

The combination of solutions of $CuBr_2$, H_2L^z, and a base resulted in the precipitation of $Cu(L^z)$. A polymeric chain structure has been proposed by Ryabukhin for this compound.[21] The green solid redissolved in boiling pyridine, and addition of MeOH and water resulted in the deposition of green crystals with the composition $[Cu(L^z)(pyridine)]_2$ (Figure 4). The dimeric complex is centrosymmetric; the two Cu^{II} cations have a slightly distorted square-pyramidal coordination geometry. The basal plane is defined by the O−N−O donor set of L^z and the pyridine *N* donor *trans* to the triazole nitrogen atom. Two $[Cu(L^z)(pyridine)]$ units are paired by mutual bridging through a coordinated phenoxo group. This phenoxo bridge represents the apex of the CuN_2O_3 pyramid. The Cu−O bond lengths fall in expected ranges.[26] However, it is interesting to note that the two Cu−N lengths (1.935 and 2.052 Å) differ significantly, the distance to the pyridine donor being longer. The bridging interaction of the phenoxo group is asymmetric with a long Cu−O distance to the donor in apical position. The two phenoxo moieties are again twisted with torsional angles of 19.2° and 24.0°. The structure is stabilized by some stacking interactions between the triazole and the pyridine moieties. As expected, the dimeric complex shows antiferromagnetic coupling between the two Cu^{II} centers with an $S = 0$ ground state.

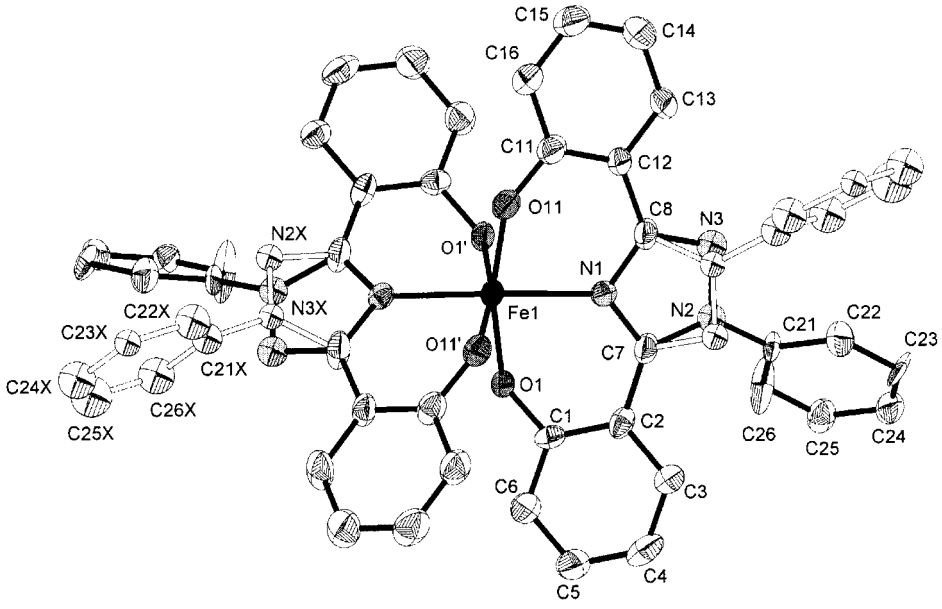

Figure 3. Molecular structure of the $[Fe(L^z)_2]^-$ anion, showing the major and minor components of the disordered structure; the atomic displacement ellipsoids are drawn at the 30% probability level; hydrogen atoms are omitted for clarity; selected bond lengths [Å] and angles (°): Fe1−O11 1.958(4), Fe1−O1 2.002(4), Fe1−N1 2.092(5), O11−Fe1−O11′ 92.4(3), O11−Fe1−O1 166.5(2), O11−Fe1−O1′ 90.6(2), O1−Fe1−O1′ 89.7(2), O11−Fe1−N1 84.1(2), O11−Fe1−N1′ 101.0(2), O1−Fe1−N1 82.4(2), O1−Fe1−N1′ 92.5(2), N1−Fe1−N1 172.7(3)

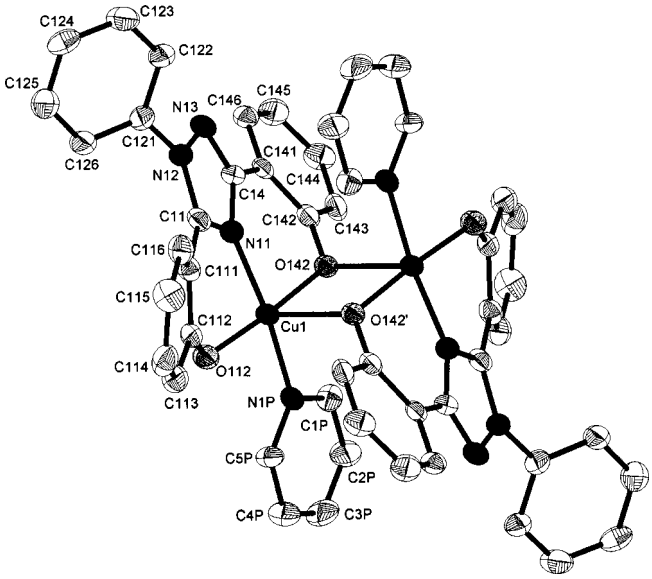

Figure 4. Molecular structure of the dinuclear $[Cu(L^z)(pyridine)]_2$ complex; the atomic displacement ellipsoids are drawn at the 30% probability level; hydrogen atoms are omitted for clarity; selected bond lengths [Å] and angles (°): Cu1−O112 1.922(6), Cu1−N11 1.935(6), Cu1−O142 1.946(5), Cu1−N1P 2.052(6), Cu1−O142′ 2.360(5), O112−Cu1−N11 89.6(2), O112−Cu1−O142 176.2(2), N11−Cu1−O142 86.8(2), O112−Cu1−O142′ 96.9(2), N11−Cu1−O142′ 96.5(2), O142−Cu1−O142′ 84.8(2), O112−Cu1−N1P 92.7(3), N11−Cu1−N1P 166.3(3), O142−Cu1−N1P 90.4(3), N1P−Cu1−O142′ 96.7(2)

2.2. pK_a Values of the Free Ligands

The pK_as were measured by potentiometric and spectrophotometric titrations (25 °C, 0.1 M KCl/KNO_3). In their fully protonated forms all three derivatives show rather low solubility in H_2O. Therefore, some of the deprotonation studies were performed in H_2O/DMSO solutions with $0.06 \leq x_{DMSO} \leq 0.20$ (x_{DMSO} is the mol fraction of DMSO). The dependence of the pK_as on x_{DMSO} was found to be roughly linear (Figure 5), and some of the missing values for pure H_2O could be estimated by extrapolation: $pK_{a,i}(x > 0) = pK_{a,i}(x = 0) + a \times x$, with $4.7 < a < 7.4$. Inspection of these data (Table 1) showed no significant differences for $pK_{a,2}$ and $pK_{a,3}$ between the three ligands H_3L^x, H_3L^y and H_2L^z. Moreover, the influence of the inert electrolyte (KCl or KNO_3) appears to be negligible, and the interpolation procedure yielded reliable estimates for the pK_as in H_2O, with an accuracy of about ±0.1. For an appropriate interpretation of these data, it is important to note that the ionic product (apparent $K_w = Q_c = [H^+] \times [OH^-]$) in the H_2O/DMSO system is considerably smaller than in pure H_2O.[27] As a consequence, the pH scale for $x_{DMSO} = 0.2$ is extended to a range of 0−15.6, and neutral solutions have a pH value of about 7.8.

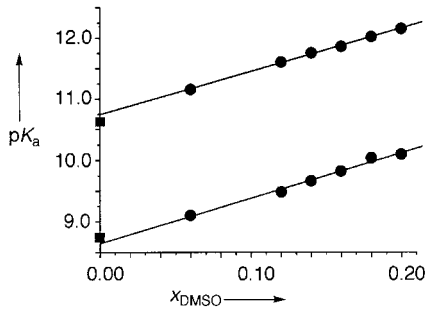

Figure 5. The dependence of the $pK_{a,2}$ and $pK_{a,3}$ of H_3L^y on x_{DMSO}; circles indicate values with $x_{DMSO} \geq 0.06$, squares refer the experimental values in pure water; the fitted line illustrates the reliability of the extrapolation procedure ($x_{DMSO} \rightarrow 0$) with an accuracy of the $x_{DMSO} = 0$ values of about ±0.1

The observed pK_a values can be grouped in three categories:

(a) $pK_a < 2$. Such low values could not be determined by conventional potentiometric methods and were therefore measured spectrophotometrically. All the investigated ligands showed significant spectral changes in the range $0 < pH < 2$. A ^1H NMR spectroscopic study of H_3L^x showed considerable shifts for the hydrogen atoms of the two phenol rings, whereas the resonances for the C_6H_4−COO hydrogen atoms (which appeared as a characteristic AA′XX′ spin system) remained virtually constant. Obviously, these changes must be attributed to protonation of a triazole nitrogen atom (for the unsubstituted 1,2,4-triazole, a pK_a of 2.19 is reported in the literature).[28] According to the ^1H

Table 1. pK_a values (25 °C, 0.1 M KCl or KNO_3) of H_3L^x, H_3L^y, and H_2L^z in H_2O and in H_2O/DMSO solutions with a mol fraction $x_{DMSO} = 0.2$; uncertainties (3σ) are given in parentheses

	H_3L^x (ICL670)		H_3L^y			H_2L^z	
	$x_{DMSO} = 0.20$						
$pK_{a,1}$[a]	4.61(2)[b] [c]	4.61(4)[d] [e]	<2				
$pK_{a,2}$[a]	10.12(2)[b][c]	10.00(3)[d][e]	10.10(4)[d][e]			10.12(1)[c][d]	10.0(1)[d][e]
$pK_{a,3}$[a]	12.08(2)[b][c]	12.12(4)[d][e]	12.15(2)[d][e]			12.21(3)[c][d]	12.2(1)[d][e]
	H_2O only						
$pK_{a,1}$[a]	−[f]	3.7(1)[d][g]	<2[c][d]	1.1(1)[d][e]			
$pK_{a,2}$[a]	8.80(1)[d][h]	9.0(1)[d][g]	8.74(1)[c][d]	8.76(3)[d][e]	8.6[d][g]	−[f]	
$pK_{a,3}$[a]	10.61(1)[d][h]	10.6(1)[d][g]	10.63(1)[c][d]	10.67(3)[d][e]	10.7[d][g]	−[f]	

[a] $pK_{a,i} = -\log K_{a,i}$, $K_{a,i} = [H_{3-i}L] \times [H] \times [H_{4-i}L]^{-1}$. [b] 0.1 M KNO_3. [c] pH titration of H_mL with KOH. [d] 0.1 M KCl. [e] Spectrophotometric titration. [f] Insufficient solubility. [g] Extrapolated for $x_{DMSO} \rightarrow 0$. [h] pH titration of $L^{x\,3-}$ with HCl.

NMR spectroscopic characteristics, protonation of the nitrogen atom is also observed for the sulfonic acid derivative H_3L^y. Consequently, H_3L^y must be present predominantly in a zwitterionic form in strongly acidic aqueous media (Scheme S1, Supporting Information).

(b) $3 < pK_a < 5$ was only observed for H_3L^x and corresponds to the deprotonation of the carboxylic acid group.

(c) $pK_a > 8$. These values are characteristic of the deprotonation of the phenolic OH groups. Although the two OH groups are structurally inequivalent, it appears highly probable that they are deprotonated simultaneously, and that the observed pK_as represent averages of the individual (microscopic) acidity constants.[29]

2.3. Complex Formation with Fe^{III}

The formation of Fe^{III} complexes with H_3L^x, H_3L^y and H_2L^z was also studied in H_2O/DMSO by potentiometric and spectrophotometric methods. The overall stability constants, which are defined according to: $mFe^{3+} + nL^{u-} + qH^+ \rightleftarrows Fe_mL_nH_q^{3m-un+q}$, $\beta_{mnq} = [Fe_mL_nH_q^{3m-un+q}] \times [Fe^{3+}]^{-m} \times [L^{u-}]^{-n} \times [H^+]^{-q}$, ($L^x$, L^y: $u = 3$, L^z: $u = 2$), are summarized in Table 2.

In acidic solution (pH <3.5), formation of a 1:1 complex was verified by Job′s plots and was further confirmed by spectrophotometric batch titrations for all three ligands (Figures S5−S7, Supporting Information). Below pH 4, ICL670 forms a protonated complex $[Fe(HL^x)]^+$ (indicated as 111 in Scheme 2). This species could be deprotonated to $[Fe(L^x)]$ (110). We propose that the additional proton is bonded to the peripheral carboxylate group of the ligand. This assignment is consistent with the observation that a corresponding 111 species does not form with the sulfonic acid H_3L^y and the phenyl derivative H_2L^z. Clearly, the peripheral sulfonate group of H_3L^y is not sufficiently basic

Table 2. Overall formation constants (log β_{mnq}) of Fe^{III} complexes with H_3L^x, H_3L^y, and H_2L^z (25 °C, 0.1 M KCl or KNO_3) in H_2O or in H_2O/DMSO solutions with a mol fraction $x_{DMSO} = 0.20$; uncertainties (3σ) are given in parentheses

log β_{mnq}[a]	H_3L^x (ICL670)	H_3L^y	H_2L^z
mnq	$x_{DMSO} = 0.20$		
111	27.5(1)[b][c]		
110	23.33(3)[d][e], 23.5(1)[b][c]	22.50(1)[b][c]	22.85(1)[b][c]
122	48.7(1)[d][e]		
121	44.36(1)[d][e], 44.5(1)[b][c]	43.05(6)[b][c]	not determined[f]
120	38.56(2)[d][e], 38.6(1)[b][c]	37.46(9)[b][c]	not determined[f]
	H_2O only		
111	24.3[b][g]		
110	22.0[b][g]	21.30(4)[b][c], 21.2[b][g]	not determined[f]
122	43.4[b][g][h]		
121	41.2[b][g]	40.89(3)[b][e], 40.79(4)[b][c], 40.9[b][g]	not determined[f]
120	36.9[b][g]	35.95(5)[b][e], 36.06(4)[b][c], 35.8[b][g]	not determined[f]

[a] $\beta_{mnq} = [Fe_mL_nH_q] \times [Fe]^{-m} \times [L]^{-n} \times [H]^{-q}$. [b] 0.1 M KCl. [c] Spectrophotometric titration. [d] 0.1 M KNO_3. [e] Potentiometric titration. [f] Insufficient solubility. [g] Extrapolated for $x_{DMSO} \rightarrow 0$. [h] This species does not appear in the equilibrium in pure H_2O to a significant extent.

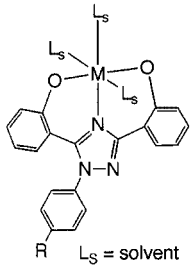

110: R = COO^-, SO_3^-, H
111: R = COOH

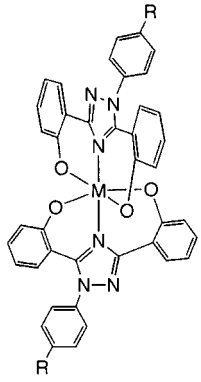

120: R = COO^-, SO_3^-, H

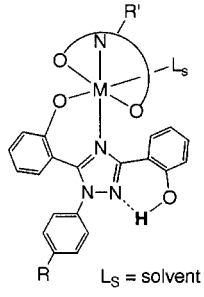

121: R = R' = COO^-, SO_3^-, H
122: R = COO^-, R' = COOH

Scheme 2

to allow protonation in aqueous solution. Moreover, $[Fe(HL^x)]^+$ and $[Fe(L^x)]$ have very similar optical spectra (Figure 6b). Since the observed bands in the Vis spectra are mainly charge-transfer transitions, protonation of the peripheral carboxylate group does not modify the chromophore of this complex to a significant extent.

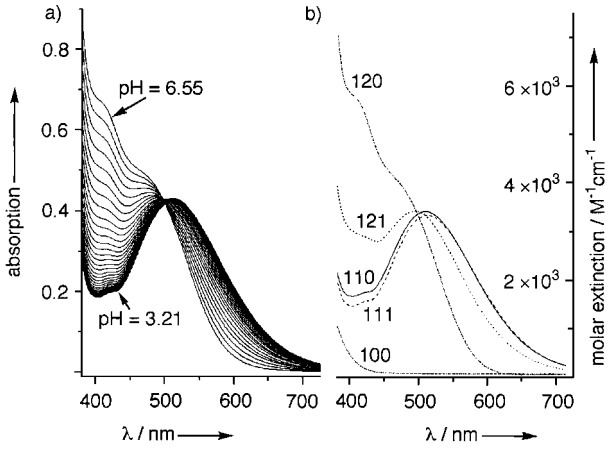

Figure 6. Determination of the formation constants log β_{mnq} of $[Fe_m(L^x)_nH_q]^{3m-3n+q}$; a) the sample spectra of the spectrophotometric titration with total [Fe]:total [L^x] = 1:3 in the range 3.2 < pH < 6.6 (x_{DMSO} = 0.2); b) calculated spectra of the individual $[Fe_m(L^x)_nH_q]^{3m-3n+q}$ species indicated as *mnq*; the spectra of Fe^{3+} (= 100) and of $[Fe(HL^x)]^+$ (= 111) were measured separately and were imported without refinement

At higher pH, complex formation with H_3L^x and H_3L^y was explored by continuous titrations (Figure 6). An additional ligand is bound to the metal center above pH 4, and a series of 1:2 complexes are formed. Experiments with H_2L^z could not be evaluated due to precipitation. Formation of a reddish-violet solid was always observed, even if a very low concentration of total Fe (10^{-4} M) and a large excess of ligand (total L^z: total Fe > 4) was used. The precipitation began after addition of about 1.2 equivalents of base, and the precipitate redissolved completely above pH 6. Obviously, a bis complex of zero charge is formed with a tentative composition $[Fe(L^z)(HL^z)]$ (indicated as 121 in Scheme 2). Formation of a similar 121 intermediate was also established for the sulfonic acid H_3L^y by potentiometric and spectrophotometric methods. However, due to the anionic nature of $[Fe(L^y)(HL^y)]^{2-}$, an insoluble solid did not form. The 121 complex deprotonated around pH 5−6 to form $[Fe(L^y)_2]^{3-}$ (= 120), which was then present as the sole species up to pH 12. The carboxylic acid H_3L^x behaved similarly, although an additional doubly protonated bis complex $[Fe(HL^x)_2]^-$ (= 122) was detected as a minor species in the region 4 < pH < 5.

For the mono complex, the reaction $[Fe(L^x)] + H^+ \rightarrow [Fe(HL^x)]^+$ was attributed to a simple protonation of the peripheral carboxylate group (vide supra). However, for the bis complexes, a different type of reaction must be considered, since $[Fe(L^y)_2]^{3-}$ and $[Fe(L^z)_2]^-$ have no peripheral sites available for protonation around pH 5 (Figure 7). Conclusive evidence for the nature of this complex is obtained from an analysis of the Vis spectroscopic data, which established that the spectra of $[Fe(L^x)(HL^x)]^{2-}$ (121) and $[Fe(L^x)_2]^{3-}$ (120) are distinctly different (Figure 6b). The situation is similar for $[Fe(L^y)(HL^y)]^{2-}$ and $[Fe(L^y)_2]^{3-}$ (see Figure S8, Supporting Information). Obviously, the two complexes must have different coordination spheres, and we therefore propose a bidentate coordination mode for one of the ligands in the 121 complex with the triazole nitrogen and one of the phenolic oxygen donors as the only coordinating atoms (Scheme 2). The second phenolic oxygen donor is protonated and probably hydrogen bonded to the free triazole nitrogen atom (as observed for the free ligands, see Figure 2). Further evidence for this particular structure is provided by FAB^+ MS (measured in EtOH). The spectrum shows the formation of the species $[Fe(L^z)_2(EtOH)]^+$ with rather high intensity. The binding of one (and only one) EtOH molecule can be nicely explained, if the complex is formulated as $[Fe(L^z)(HL^z)OEt]^+$, with a bidentate HL ligand and the sixth position in the coordination sphere occupied by an OEt^- moiety.

The spectra of the monoprotonated $[Fe(L^x)(HL^x)]^{2-}$ and the doubly protonated $[Fe(HL^x)_2]^-$ do not differ to any significant extent, and we therefore assign the reaction of $[Fe(L^x)(HL^x)]^{2-}$ with H^+ to a simple protonation of one of the peripheral carboxylate groups. The similarity of the two spectra, together with a rather low abundance of these species, prevents the determination of the formation constant β_{122} of $[Fe(HL^x)_2]^-$ by spectrophotometric methods. The value for log β_{122} could only be established by potentiometric titrations. In agreement with this assignment, the doubly protonated $[Fe(HL^y)_2]^-$ and $[Fe(HL^z)_2]^+$ species were not observed.

A comparison of the various log β values (Table 2) shows the following trends:

(a) *Dependence on DMSO concentration.* The sulfonic acid derivative has significantly enhanced solubility, and the entire range $0 \le x_{DMSO} \le 0.2$ could thus be investigated. A steady increase of log β was generally noted for an increase in the mol fraction of DMSO. The difference $\Delta\log\beta = \log\beta_{x(DMSO)=0.2} - \log\beta_{x(DMSO)=0}$ is 1.2 for $[Fe(L^y)]$, and 1.5 for $[Fe(L^y)_2]^{3-}$. Complex formation of H_3L^x with Fe^{3+} was performed in solutions with a mol fraction x_{DMSO} of 0.22, 0.20 and 0.18. The extrapolation $x_{DMSO} \rightarrow 0$ yielded $\Delta\log\beta_{110}$ = 1.3 and $\Delta\log\beta_{120}$ = 1.6. The similar behavior of the two ligands H_3L^x and H_3L^y and the linear dependence of log β on x as observed for H_3L^y justify application of the extrapolation procedure as described above for the pK_a values (Figure 5). As a result, we note that $Fe^{III}-L^x$ complexes with a peripheral COOH group are much stronger acids in H_2O than in H_2O/DMSO mixtures. Corresponding pK_a values derived from the overall formation constants (Table 2) are 2.3/2.2 (H_2O) and 4.2/4.3 (x_{DMSO} = 0.2) for $[Fe(HL^x)]^+$/$[Fe(HL^x)_2]^-$. We attribute this effect to the different solvation properties of the two media. Consequently, such protonated species appear in a substantial amount in the H_2O/DMSO mixture (Figure 7a), whereas in pure H_2O, their formation is of minor relevance or not significant at all (Figure 7b).

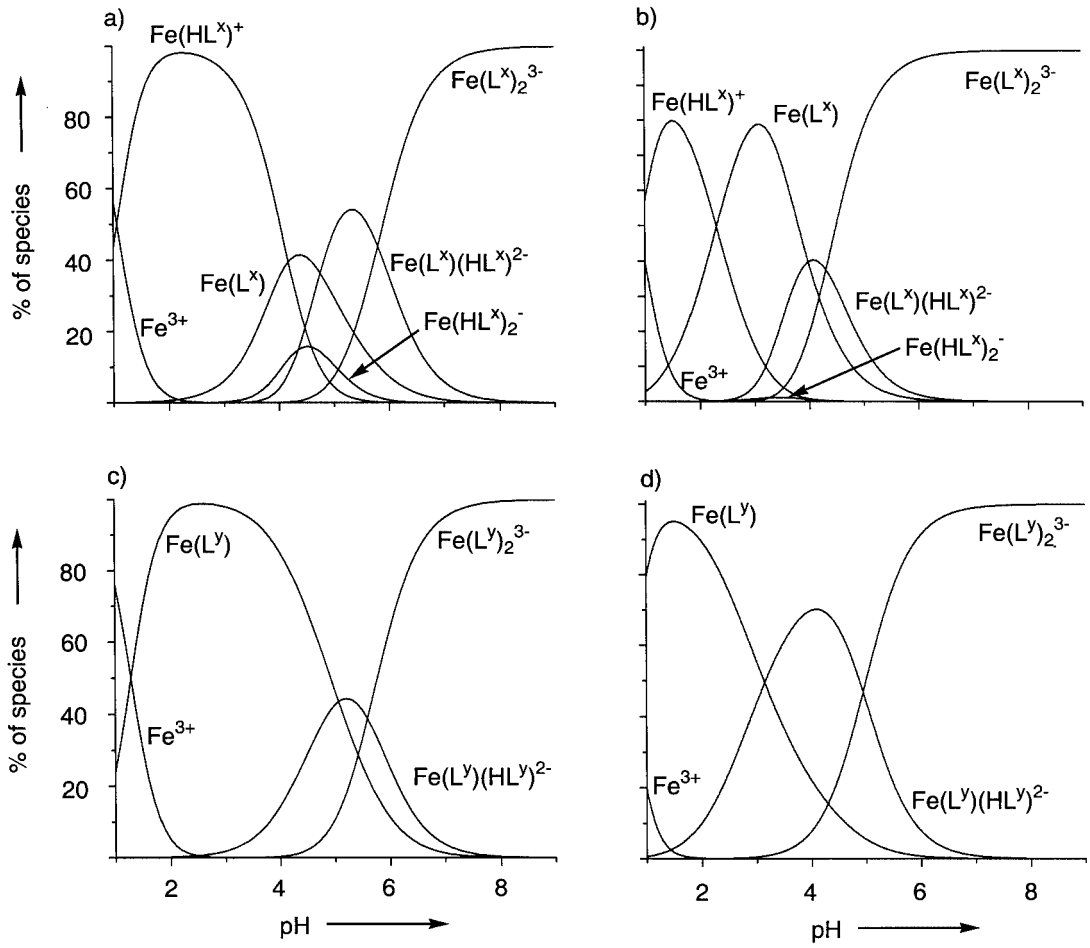

Figure 7. Species distribution plots for equilibrated solutions of $Fe^{III}-H_3L$ systems; a) H_3L^x, $x_{DMSO} = 0.2$; b) H_3L^x, $x_{DMSO} = 0.0$; c) H_3L^y, $x_{DMSO} = 0.2$; d) H_3L^y, $x_{DMSO} = 0.0$; total Fe and total ligand concentrations are 1.0 mM, and 2.0 mM, respectively; only metal-containing species are shown (total Fe = 100%); the equilibrium constants listed in Tables 1 and 2 were used for the calculations

(b) *Comparison of the different ligands.* The stability of [FeL] with $x_{DMSO} = 0.2$ decreases in the order $H_3L^x > H_2L^z > H_3L^y$. However, the differences are relatively minor. In general, the iron binding properties of H_3L^x and H_3L^y are indeed closely related: the pFe values[30] for H_3L^x and H_3L^y (total [L] = 10 μM, total Fe = 1 μM, pH = 7.4, H_2O, $I = 0.1$ M) are 21.5 and 20.6, respectively.

2.4. Complex Formation with Fe^{II}

The formation of Fe^{II} complexes with H_3L^y was again studied in H_2O/DMSO mixtures ($x_{DMSO} = 0.20$). However, a quantitative determination of the formation constants proved extremely difficult, because the ferrous complexes reacted as strong reducing agents and were readily oxidized to the corresponding Fe^{III} species. This oxidation process could easily be observed by the intense red or purple color of the Fe^{III} complexes (the Fe^{II} complexes are virtually colorless). It was thus of utmost importance to remove any traces of oxygen from the sample solutions. A series of potentiometric titrations was performed under Ar to determine the corresponding formation constants. However, it was not possible to suppress the oxidatively induced side reactions completely. In particular, the 1:2 complex $[Fe^{II}(L^y)_2]^{4-}$ was found to be a strong enough reducing agent to be oxidized even in the complete absence of oxygen. Corresponding CV measurements (see section 2.5.2) confirmed that $[Fe^{II}L_2]^{4-}$ is able to reduce H_2O (formation of H_2) in neutral solution. It was therefore not possible to determine any formation constant for the ferrous 1:2 complex with this method. The potentiometric measurements could, however, be used to investigate the formation of the 1:1 complex $[Fe^{II}(L^y)]^-$, according to the reaction $Fe^{2+} + H_3L^y \rightleftarrows [Fe(L^y)]^- + 3\ H^+$. The overall formation constant β_{110} (referring to the reaction $Fe^{2+} + L^{3-} \rightleftarrows [FeL]^-$) was determined in H_2O/DMSO ($x_{DMSO} = 0.2$) to be $\log \beta_{110} = 11.5(2)$. As expected, this number is substantially lower than the corresponding value for Fe^{3+} (22.5, see Table 2).

2.5. Redox Properties of the $Fe^{II}/Fe^{III}-H_3L$ System

2.5.1. Redox Chemistry in Acidic Solutions

Below pH 3, the 1:1 complexes $[Fe(HL^x)]^+$ and $[Fe(L^y)]$ are predominantly formed, even when the ligand is present in excess (Figure 7). The redox characteristics of these two complexes have been investigated thoroughly by means of cyclic voltammetry. The two complexes behave rather similarly, and we will focus here on the behavior of $[Fe(HL^x)]^+$ (Figure 8) and present the results for $[Fe(L^y)]$ in an abbrevi-

ated manner. A Pt working electrode was used exclusively in acidic solution, and all experiments were performed in a H_2O/DMSO medium ($x_{DMSO} = 0.2$) to avoid precipitation of the insoluble H_3L. The use of DMSO as a particularly useful solvent in electrochemistry is well-established.[31]

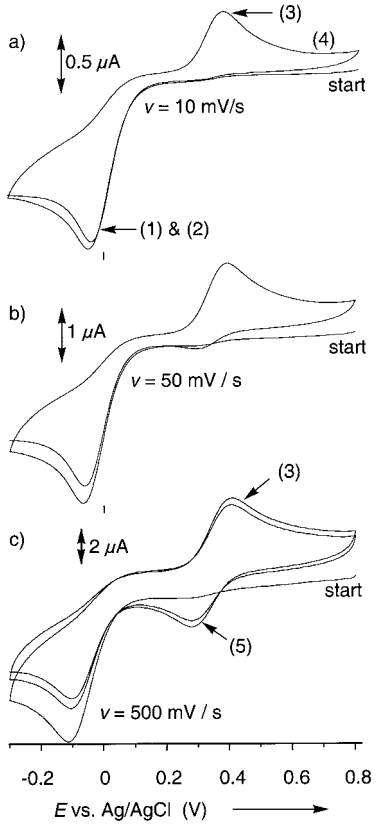

Figure 8. Cyclic voltammograms of $[Fe(HL^x)]^+$ (pH = 2.9, total [Fe] = 2.5 mM, total [L^x] = 5 mM, $x_{DMSO} = 0.2$ using a Pt working electrode at scan rates as indicated

Reduction of $[Fe(HL^x)]^+$ resulted in the formation of the corresponding Fe^{II} complex according to the reaction:

$$[Fe^{III}(HL^x)]^+ + e^- \rightarrow [Fe^{II}(HL^x)] \quad (1)$$

However, the ferrous complex is not stable and decomposes immediately and completely according to the reaction:

$$[Fe^{II}(HL^x)] + 2\,H^+ \rightarrow Fe^{2+} + H_3L^x \quad (2)$$

The electron uptake and complex decomposition described by the above reactions [Equation (1) and Equation (2)] was indicated by a characteristic irreversible peak in the range +100 mV to −150 mV (versus Ag/AgCl). As indicated by Equation (2), the decomposition is strongly pH dependent. The peak shifted to less positive values at higher pH with a slope of 109 mV/pH ([Fe(L^y)]: 129 mV/pH), indicating a transfer of two protons per electron (Figure S13, Supporting Information). The cathodic peak current was found to be linearly dependent on the square root of the scan rate, as expected for a diffusion controlled reaction (Figure S12, Supporting Information). The peak potential of the reduction slightly shifted to less positive values with increasing scan rate, and this is consistent with an irreversible process. As a result of the complete decomposition of the complex, the reverse scans showed a half wave indicative of the reoxidation of the free Fe^{2+} to Fe^{3+} at about 400 mV (versus Ag/AgCl) according to:

$$Fe^{2+} \rightarrow Fe^{3+} + e^- \quad (3)$$

This assignment is further supported by a characteristic time dependence, which was observed in subsequent scans. If a sufficiently slow scan rate was used (< 50 mV/s), enough time was available for the re-formation of the ferric complex after reoxidation of Fe^{2+} to Fe^{3+}, according to:

$$Fe^{3+} + H_3L^x \rightarrow [Fe^{III}(HL^x)]^+ + 2\,H^+ \quad (4)$$

Consequently, the second scan was identical to the first scan. Further scans did not result in any change in the behavior. However, if a higher scan rate of about 50−500 mV/s was applied, $[Fe^{III}(HL^x)]^+$ was only partially recovered [Equation (4)], and in the following scan, the solution still contained some free Fe^{3+}, which was reduced to Fe^{2+}:

$$Fe^{3+} + e^- \rightarrow Fe^{2+} \quad (5)$$

The above reaction [Equation (5)] resulted in the appearance of a new reduction wave at around 300 mV (versus Ag/AgCl), and as a consequence, two reduction waves [see Equation (1) and Equation (5)] were now observable. The ratio of their intensity varied characteristically with scan rate. Increasing scan rates resulted in an increase in the suppression of Equation (4), and therefore in an increase in the amount of free Fe^{3+} and a decrease in the amount of $[Fe^{III}(HL^x)]^+$. Consequently, the intensity of the peak at 300 mV increased with increasing scan rate, whereas that of the peak at around −100 mV (its counterpart) diminished. At a scan rate higher than 500 mV/s, the amount of complex formed after the first cycle was less than 50%, and the quasi-reversible pattern for the free Fe^{2+}/Fe^{3+} couple [Equation (3) and Equation (5)] was observed. This time-dependence was found to be in good agreement with the kinetics of $[Fe(HL^x)]^+$ formation, which was established previously by stopped flow experiments.[17]

If the pH was lowered to ≤2, the acidity of this medium was high enough to lead to the partial decomposition of $[Fe^{III}(HL^x)]^+$ (Figure 7):

$$[Fe^{III}(HL^x)]^+ + 2\,H^+ \rightarrow Fe^{3+} + H_3L^x \quad (6)$$

Consequently, two reduction waves were observed already in the first scan, and it was not possible to suppress the peak at 300 mV by sufficiently slow scan rates.

2.5.2. Redox Chemistry in Neutral and Alkaline Solutions

Above pH 6, 1:2 complexes are predominantly formed, and the relevant reduction reaction is thus:

$$[Fe^{III}(L)_2]^{3-} + e^- \rightarrow [Fe^{II}(L)_2]^{4-} \quad (7)$$

However, CV experiments with an Au, Pt or glassy carbon working electrode did not show any redox activity for $[Fe^{III}(L)_2]^{3-}$. Obviously, $[Fe^{II}(L)_2]^{4-}$ is a stronger reducing agent than H_2 (see section 2.4), and the failure to observe any redox activity is due to the production of hydrogen prior to the reduction of the complex. An Hg (hanging drop) electrode was thus used to circumvent the problem of hydrogen formation, and the quasi-reversible reduction of $[Fe^{III}(L)_2]^{3-}$ [Equation (7)] could then be detected above pH 12 (Figure 9). The peak separations ΔE_P were 93 mV and 102 mV, and the reduction potentials for the $[Fe^{III/II}(L)_2]^{3-/4-}$ couple were −0.92 V and −0.89 V for H_3L^x and H_3L^y, respectively (x_{DMSO} = 0.2, vs. Ag/AgCl). As expected, this value does not depend on pH (Figure S14). Plots of the cathodic peak current vs. the square root of scan rate established a purely diffusion-controlled process (Figure S12). At pH <12, the two waves of to this redox process were still visible; however, additional peaks were observed in the reverse scan at more positive values (Figure S15). We attribute these characteristics to a partial dissociation of the ferrous complex [Equation (8)]:

$$[Fe^{II}L_2]^{4-} + nH^+ \rightarrow [Fe^{II}L]^- + H_nL^{n-3} \quad (8)$$

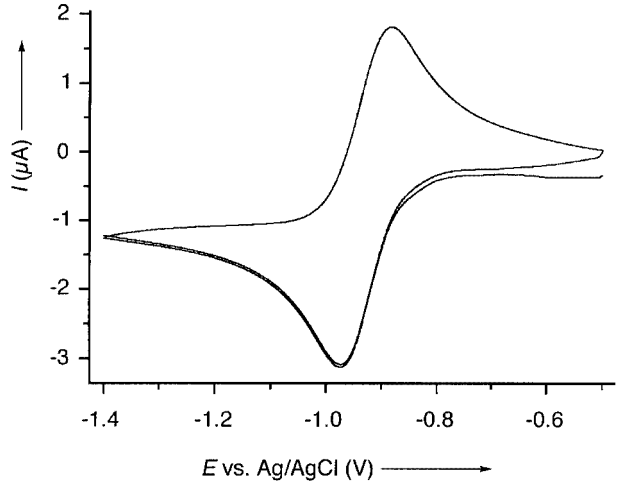

Figure 9. Cyclic voltammogram of $[Fe(L^x)_2]^{3-}$ (pH = 12.7, total [Fe] = 2.5 mM, total [L^x] = 5 mM, x_{DMSO} = 0.2 at a Hg (hanging drop) working electrode with a scan rate of 50 mV/s

For ICL670 (H_3L^x), the reduction of $[Fe^{III}(L)_2]^{3-}$ [Equation (7)] was also investigated in H_2O, and a very similar behavior was noted. The observed reduction potential was determined as −0.58 V (versus NHE). Excess ligand was used as buffer in our aqueous experiments, to stabilize the pH in the range 11−12 (the free ligand is electrochemically inactive). Moreover, the excess ligand also inevitably served to suppress the decomposition of $[Fe^{II}L_2]^{4-}$ [Equation (8)].

3. Discussion

3.1. Structure and Selectivity

It has been suggested that the application of ICL670 in the therapy of iron overload could be problematic due to the lack of sufficient selectivity.[2] In particular, the presence of an sp^2 nitrogen atom would generate a donor set with a significant tendency to bind divalent biometal cations such as Zn^{2+}. Although the affinity of high-spin Fe^{III} for six negative oxygen donors generally appears to be overestimated,[32] it is true that an increasing number of nitrogen donors would enhance the stability of metal complexes with late divalent transition metal cations (Ni^{2+}, Cu^{2+}, Zn^{2+}), because an sp^2 nitrogen donor is somewhat softer than a negative oxygen donor.[33,34] However, the metal selectivity of a complexing agent cannot be explained simply in terms of the hardness of the donor set. Additional steric factors of the ligand must also be considered,[33] and it appears that in discussing the metal-ion selectivity of ICL670, these steric aspects have not received the necessary attention in some of the previous reports.

With regard to the particular steric properties of ICL670, it is important to recognize that an entirely planar L−M unit with an O−M−O angle of 180° (Scheme 3a) would imply an M−O bond length of 1.60 Å and an M−N bond length of 1.90 Å. Only very small cations are capable of forming such a short M−O bond. It has been shown by Hancock that ligands forming six-membered chelate rings have a distinct preference for small metal centers, whereas five-membered chelate rings are more suited for larger cations.[35] Clearly, with its rigid structure and its constraint of two six-membered chelate rings, ICL670 will have a strong preference to bind small metal cations. As a consequence, *all* complexes of ICL670 with di- and trivalent transition-metal cations must be regarded as strained, and this strain increases significantly with increasing ionic size. This result is of importance with regard to selectivity of this ligand in biological systems. It is noteworthy that most of the competing biometal cations such as Zn^{2+} are larger than Fe^{3+}, and binding of these elements to ICL670 is thus clearly discriminated on the basis of steric considerations. The bond strain in such complexes can be absorbed to a large extent by angle deformation, and the M−O distance can be widened by out-of-plane twisting of the two phenyl rings (Scheme 3b). As already noted in the results section (2.1.2), this type of twist has generally been observed in the crystal structures of such metal complexes, and the corresponding twist angle increases, as expected, with increasing ionic ra-

dius. However, the rotation of the two phenoxo rings inevitably results in a compression of the M−N bond. Corresponding M−N distances observed in the crystal structures are indeed rather short. Again, the compression is partially compensated by deformation of the *cis*−O−M−N and *trans*−O−M−O angles (Scheme 3c).

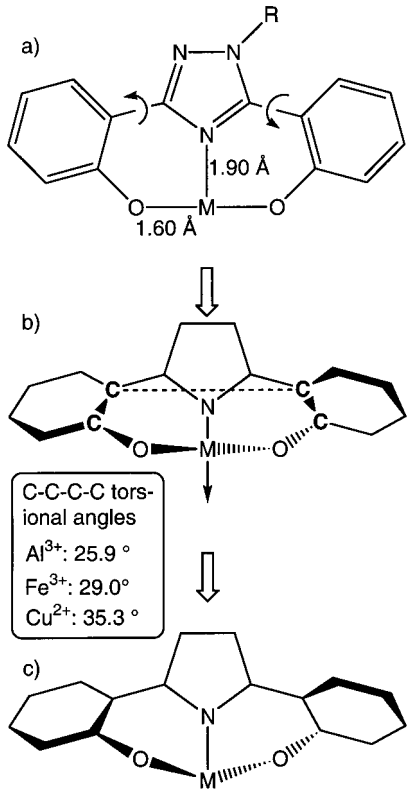

Scheme 3

The favored binding of small metal cations is nicely illustrated by the stability constants of $[M(L^x)]$ complexes with Mg^{2+} (log K = 7.6) and Ca^{2+} (log K = 5.5).[17] These values should be compared with values for other ligands that have a mixed *O*,*N* donor set such as NTA^{3-} (log K_{MgNTA} = 5.5, log K_{CaNTA} = 6.3) or EDTA (log K_{MgEDTA} = 8.8, log K_{CaEDTA} = 10.7).[36] The two aminopolycarboxylate ligands exclusively form five-membered chelate rings, and as a consequence, the complexes with the larger cation (Ca^{2+}) are more stable. For ICL670, the reverse trend is observed, and the complexes with the smaller Mg^{2+} are about two orders of magnitude more stable. Consequently, replacement of the ferric iron by the larger Zn^{2+} ion, according to $[Fe(L^x)_2]^{3-} + Zn^{2+} \rightleftarrows [Zn(L^x)_2]^{4-} + Fe^{3+}$, is strongly disfavored. The equilibrium constant for this reaction is 7.9×10^{-22}.[17] The significant stress, even in the ferric complex, also explains the rather unexpected formation of the protonated species $[Fe(L)(HL)]^{2-}$ (L = L^x, L^y) or [Fe(L)(HL)] (L = L^z) that was observed for all three ligands. Obviously, the transformation to a bidentate coordination mode arises because of the release of strain induced by the detachment of one of the coordinated phenoxo groups. Such a detachment of a basic donor atom by protonation is well-established for strained chelate rings.[37]

In the bis complexes of ICL670, the discussion of structure-stability correlations requires the analysis of additional interligand interactions. For this purpose, it is necessary to briefly discuss the different stereoisomers that are possible for such an ML_2 complex. In the simple ML unit, the twist of the two phenyl rings can either occur in a clockwise or counter-clockwise manner relative to the central triazole unit (Scheme 4a). By analogy with the usual nomenclature, the O···O line will be used in this work to refer to the two forms as the λ or δ enantiomer, and the combination in a bis complex would give either a λδ or a δδ (or λλ) form (Scheme 4b). The two forms adopt considerably different geometries. In the λδ isomer, the two ligands are oriented perpendicularly, whereas the δδ isomer has a rather flat shape with an almost parallel orientation of the four phenyl rings that allow for some π-stacking to occur. Due to the nonequivalence of the two noncoordinating nitrogen atoms, the symmetry of the λδ isomer is C_1. For the δδ isomer, the addition of a substituent to one of the nitrogen atoms results either in a *cisoid* or *transoid* structure. Both of these have C_2 symmetry. $[Fe^{III}(L^z)_2]^-$ and $[Al^{III}(L^z)_2]^-$ − as observed in the crystalline compounds − correspond to the C_2 isomer with the transoid configuration being predominant (Figure 3). Inspection of the different structures reveals that for all possible isomers, *repulsive* interligand interactions are relatively minor. The exclusive formation of the λλ/δδ form in the Fe^{III} and Al^{III} complexes may be attributed to the possible stabilization by intramolecular π-stacking and also to the better accessibility of the Na^+ counterion for its bonding to two phenoxo oxygen atoms (indicated by arrows in Scheme 4b).

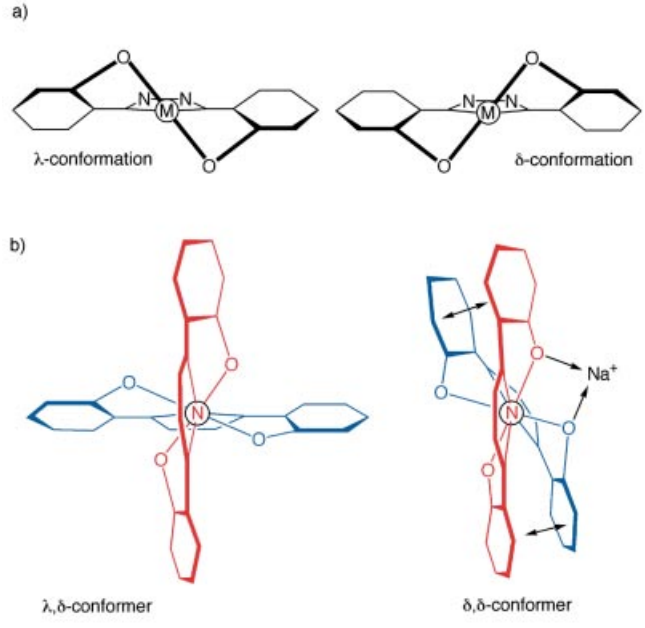

Scheme 4. a) The two enantiomeric ML conformations; b) the possible ML_2 forms (λ,δ and δ,δ)

3.2. Species Distribution and Redox Properties of the Fe^{III}−ICL670 System

As outlined in the introduction, the abundance and redox potential of every single component must be considered when discussing the problem of possible redox cycling. As a tridentate ligand, ICL670 can form ML and ML_2 complexes, and both species must be regarded as possible redox catalysts. A conventional species distribution diagram for the ICL670−Fe^{3+} system is shown in Figure 7 (see a and b). However, in this type of representation, the amount of total Fe in solution is arbitrary. In contrast, Figure 10 illustrates a situation in which the different ferric complexes are in equilibrium with solid FeOOH. The concentration of free Fe^{3+} is then mediated by the solubility product of this solid phase, and the total amount of dissolved Fe is a direct measure of the efficacy of a ligand for Fe^{III} chelation at a given pH.[38] This type of representation more closely reflects the condition in an iron-overloaded patient. Figure 10 shows the amount of dissolved Fe for total ligand concentrations of 100 μM, 1 μM, and 10 nM (the corresponding value in the serum of an iron-overloaded patient during oral treatment with ICL670 falls in the range 10 μM−100 μM).[4] As expected, ICL670 displays optimum activity in neutral and slightly alkaline solutions ($6 < pH < 10$).[38] High concentrations of H^+ or OH^- favor either competitive protonation of the ligand or render the solid hydroxide very insoluble. At physiological conditions, more than 80% of the ligand is still loaded with Fe^{III} as $[FeL_2]^{3-}$ even at low total L concentrations such as 1 μM, and the fraction of the 1:1 complex is less than 3%, even if the level of total L is 10 nM. The protonated 1:2 complex is not of importance at physiological conditions as well.

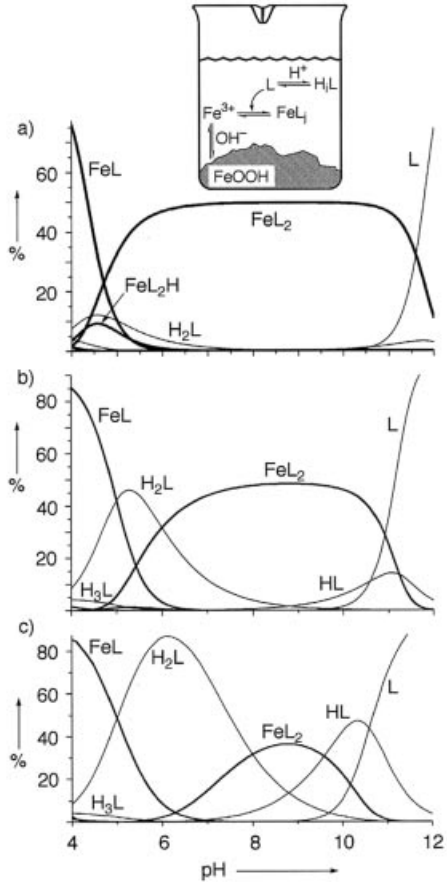

Figure 10. Sequestering ability of ICL670 in H_2O (0.1 M KCl, 25 °C) as a function of pH; the equilibrium concentration of the various species is shown as a fraction of total L concentration (= L_{tot}) with (a) L_{tot} = 100 μM, (b) L_{tot} = 1 μM, and (c) L_{tot} = 10 nM; the solubility product K_{S0}(FeOOH) = 10^{-39} M^4 corresponds to the solubility of ferrihydrite, (ref.[1]); the curves for iron-containing species are in bold

The stability of ferrous $[Fe^{II}(L^y)]^-$ (log β_{110} = 11.5) can be compared with the corresponding value log β_{110} = 13.3 reported for $[Zn(L^x)]^-$.[17] The ratio of these values corresponds closely to the expectations from a linear free energy relation $\Delta G^{Zn}/\Delta G^{Fe}$ = constant.[33] For a variety of ligands having similar, mixed *N*,*O* donor sets and a related charge or denticity, the ratio log $\beta_{110}([Zn^{II}L])$/log $\beta_{110}([Fe^{II}L])$ is 1.1−1.2 (Table 3). The corresponding ratio of 1.16 for log $\beta([Zn^{II}(L^x)]^-)$/log $\beta([Fe^{II}(L^y)]^-)$ corroborates the potentiometric results of the present investigation.[39] The value for β_{120} for the ferrous complex could not be determined directly due to instantaneous oxidation of $[FeL_2]^{4-}$. An analogous free energy relation as described for log β_{110} gave log β_{120} = 14.8 (x_{DMSO} = 0.2, see Table 3). With the use of an appropriate correction for $x_{DMSO} \rightarrow 0.0$ (Table 2), we estimate log β_{120} = 13.5 for pure water. This value is in good agreement with log β_{120} = 14.0 calculated from the reduction potential and from log β_{120} = 36.9 for $[Fe^{III}L_2]^{3-}$ (Scheme 5).

Table 3. Linear free energy relation for Zn^{2+} and Fe^{2+} complex formation

	Zn^{2+}		Fe^{2+}		log β (Zn^{2+})/log β (Fe^{2+})	
	log β_{110}	log β_{120}	log β_{110}	log β_{120}	log β_{110}	log β_{120}
$dipic^{2-}$[a]	6.35[b]	11.88[b]	5.71[b]	10.36[b]	1.11	1.15
nta^{3-} [a]	10.45[c]	14.24[c]	8.90[c]	11.98[c]	1.17	1.19
ida^{2-} [a]	6.58[d]	11.8[d]	5.45[d]	9.82[d]	1.21	1.20
L^{3-}	13.3[e]	16.0[f]	11.5[g]	14.0[h]	1.16	1.17

[a] Abbreviation of ligands: nitrilotriacetic acid (H_3nta), iminodiacetic acid (H_2ida), dipicolinic acid (H_2dipic). [b] From ref.[36], 20 °C, *I* = 0.1 M. [c] From reference [36], 25 °C, *I* = 0.1 M. [d] From ref.[36], 25 °C, *I* = 1.0 M. [e] From ref.[17], L = L^x, x_{DMSO} = 0.20, 25 °C, *I* = 0.1 M. [f] Ref.[17] listed the value log β_2 = 17.5 for L = L^x, x_{DMSO} = 0.20. This value was adjusted for pure H_2O (x_{DMSO} = 0) by adding an increment of −1.5 (see Table 2). [g] This work, L = L^y, x_{DMSO} = 0.20, 25 °C, I = 0.1 M.[h] L = L^x, estimated for H_2O (25 °C, I = 0.1 M) from the reduction potential $E_{1/2}(FeL_2)$ = −0.58 V and log β_{120} (Fe^{3+}) = 36.9 (see Scheme 5 and Table 2).

The low stability of $[Fe^{II}L_2]^{4-}$ (L = L^x, L^y) is an important result from this investigation. This complex is not only a very strong reducing agent, but also dissociates very easily to give the 1:1 complex. The individual association constant for the second ligand has a value of log $K_2 \approx 4$, and the pH-dependent constant according to Equation (8), *n* = 2, $K = [Fe^{II}L^-] \times [H_2L^-] \times [Fe^{II}L_2{}^{4-}]^{-1} \times [H^+]^{-2}$, is log *K* = −15.4. At pH 7, this equilibrium is clearly shifted to the right, and $[Fe^{II}L_2]^{4-}$ is only stable at a relatively high ligand concentration and high pH. The very low stability of

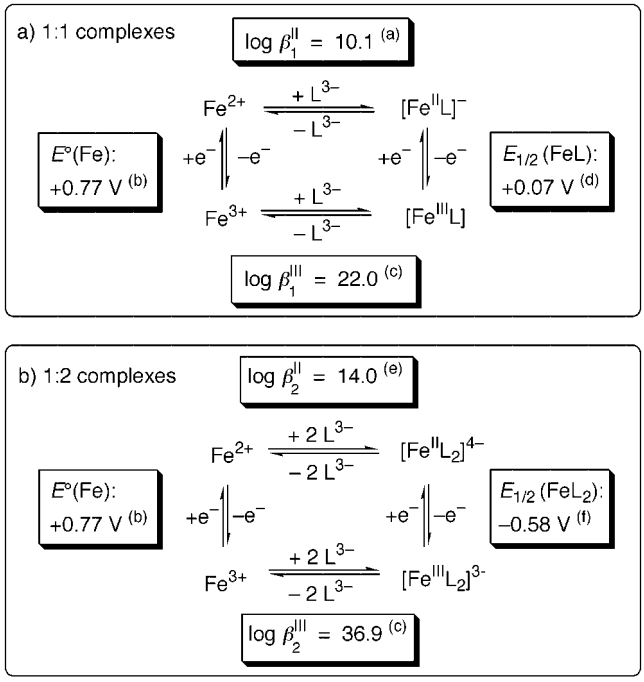

Scheme 5. Synopsis of complex stability and redox chemistry for iron complexes of H_3L^x in H_2O (0.1 M KCl, 25 °C); (a) this work (section 2.4), corrected for pure H_2O; (b) from ref.[18b]; (c) this work (see Table 2); (d) calculated as $E_{1/2}(FeL) = E^0(Fe) - 0.059V \times (\log \beta_1^{III} - \log \beta_1^{II})$; (e) calculated as $\log \beta_2^{II} = \log \beta_2^{III} - [E^0(Fe) - E_{1/2}(FeL_2)]/0.059V$; (f) this work (section 2.5.2)

the ferrous bis complex is attributed (a) to an unfavorable electrostatic repulsion between the two trianionic ligand entities, and (b) to the distinct selectivity of this ligand for small metal ions. As already discussed in section 3.1, *all* complexes of ICL670 with di- and trivalent transition metal cations must be regarded as significantly strained, and this strain increases with increasing ionic size. The addition of one electron to the ferric complex results in an increase in the effective ionic radius from 0.645 Å (high-spin Fe^{III}) to 0.780 Å (high-spin Fe^{II}).[40]

In addition to the complete dissociation of one ligand from $[Fe^{II}L_2]^{4-}$, the formation of a species with a partially coordinated and partially protonated ligand (e.g. $[Fe^{II}(L^x)(HL^x)]^{3-}$) must be taken into account. Moreover, it should be noted that $[Fe^{II}L]^-$ is susceptible to the binding of another ligating agent A^{m-} which may be present in the medium. Formation of such a ternary complex $[Fe^{II}(L^x)(A)]^{(1+m)-}$ appears to be particularly likely if this ligating agent could stabilize the ferrous form. The simple, pH-independent reduction potential [Equation (7)] must therefore be determined at a sufficiently high pH.[41] It is noteworthy that a cyclic voltammogram of the bis complex recorded at pH 12.6 showed a quasi-reversible electron transfer, whereas at lower pH, additional peaks were observed for the anodic wave at more positive potentials (Figure S15). This observation is a clear indication that additional species (protonation products of $[Fe^{II}L_2]^{4-}$ or ternary mixed ferrous complexes) are formed. However, at the present stage, it is not possible to derive any conclusive information about the nature of such species.

The formation of polynuclear species is another possibility for the stabilization of the 1:1 complex at the ferrous stage.[2] As already noted by Ryabukhin, the reaction of H_2L^z with divalent transition metal cations resulted in the precipitation of insoluble polymers.[21] A bis-bidentate coordination mode (binding of a first metal cation to N1 and O2, and a second cation to N3 and O1, see Figure 2) was proposed for the resulting $\{M(L^z)\}_n$ structure. In turn, each metal center would be chelated by two ligand entities. For H_3L^x, the corresponding oligomers $[\{Fe^{II}(L^x)\}_n]^{n-}$ would carry a negative charge at physiological pH, and they could therefore stay in solution. However, the smooth reaction of $Cu(L^z)$ with pyridine (Figure 4) demonstrates that such aggregates depolymerize readily in the presence of an additional coordinating agent.

With regard to the role of Fe^{III}−ICL670 complexes as possible catalysts for redox cycling, one can clearly state that the bis complex [Equation (7)] is redox inactive in any physiological medium. If partial dissociation and formation of the ternary $[Fe^{II}(L^x)(A)]^{(1+m)-}$ species at the ferrous stage is considered, then the result is unchanged, as long as the ligating agent A^{m-} further stabilizes the ferric form. This is indeed the case for many biological low-molecular-weight ligands such as citrate or ATP.

Although the reduction potential of $[Fe^{III}L]$ cannot be measured directly due to immediate decomposition of the complex after reduction in acidic solution (2.5.1), it can be calculated from the corresponding formation constants β_{110} for $[Fe^{II}L]^-$ and $[Fe^{III}L]$. The estimated $E_{1/2}$ for the 1:1 complex is +0.07 V (versus NHE), a value which is in good agreement with the irreversible cathodic wave (Figure 8) observed in acidic media in the range from +100 mV to −150 mV (versus Ag/AgCl). Clearly, $[Fe^{II}L]^-$ is a significantly weaker reducing agent than $[Fe^{II}L_2]^{4-}$. The redox potential of the 1:1 complex falls in a similar range to that of the $Fe^{III/II}$−EDTA couple (Figure 1).

4. Conclusions

A survey of the various formation constants and corresponding redox potentials of the Fe^{II} and Fe^{III} complexes with ICL670 (H_3L^x) in H_2O is summarized in Scheme 5. The other ligands (H_3L^y and H_2L^z) behave very similarly. Our study confirmed that these ligands are highly selective for Fe^{III}, and that the affinity for Fe^{II} is, in general, low. However, there is a distinct difference between the 1:1 and 1:2 complexes. $[Fe^{II}(L^x)]^-$ is sufficiently stable to be formed at moderate ligand concentrations around pH 6, whereas $[Fe^{II}(L^x)_2]^{4-}$ is generally not stable in aqueous solution. In view of a possible role in redox catalysis, reduction of $[Fe^{III}(L^x)_2]^{3-}$ is not possible in a physiological medium, and the 1:2 complex is thus redox inactive. On the other hand, the 1:1 complex $[Fe^{II}(L^x)]^-$ must be regarded as a somewhat milder reducing agent, and its formation from the ferric species could well be anticipated in the presence of a bio-

logical electron donor. In particular, reduction by $O_2^{\cdot-}$ could occur (Figure 1), and reoxidation by H_2O_2 would also be possible. However, the formation of $[Fe^{III}(L^x)]$ is only relevant in acidic solutions. At pH 7−8, a ligand redistribution reaction, followed by precipitation of solid iron hydroxide according to: $2[Fe^{III}(L^x)] + 3OH^- \rightarrow FeOOH(s) + [Fe(L^x)_2]^{3-} + H_2O$, would be favored (Figure 10). Therefore, it appears rather unlikely that any possible enhancement of oxidative stress (Fenton chemistry etc.) needs to be considered under physiological conditions. This is clearly different at lower pH values, where $[Fe^{III}(L^x)_2]^{3-}$ will partially dissociate to $[Fe^{III}(L^x)]$, and this species can be reduced to $[Fe^{II}(L^x)]^-$. As a matter of fact, the partial dissociation of Fe^{III} complexes in slightly acidic solutions appears to be a general problem for di- and tridentate iron chelators such as L1 or ICL670.[42] This is, of course, different for ligands with a higher denticity such as DFO, where an "all-or-nothing" coordination mode prevents possible formation of partially coordinated, "dangerous" species.

Experimental Section

Materials, Instrumentation and Analyses: The chemicals used for the synthetic work were commercially available products of reagent grade quality and were used as obtained. H_2O was distilled twice (quartz apparatus). DMSO was from Fluka (puriss., p.a.). MeOH and EtOH (reagent grade) were purified by distillation prior to use. For the potentiometric and spectrophotometric titrations, metal salts of highest available quality (>99.95%) were used. $FeCl_3$ (anhydrous) was from Fluka, $(NH_4)_2Fe(SO_4)_2{\cdot}6H_2O$ (>99.997%) from Aldrich. ^1H and $^{13}C\{^1H\}$ NMR spectra were measured in [D$_6$]DMSO (28 °C) with a Bruker DRX 500 spectrometer (resonance frequencies: 500.13 MHz for ^1H and 125.9 MHz for ^{13}C). Chemical shifts (in ppm) are given relative to tetramethylsilane as an internal standard (= 0 ppm). EI^+-MS were measured on a Varian MAT 311 spectrometer (Dr. Graf, Universität des Saarlandes), and FAB^+-MS were recorded on a VG ZAB-VSEQ spectrometer (Dr. W. Amrein, R. Häfliger, ETH Zürich). Samples for FAB were dissolved in EtOH with 3-nitrobenzyl alcohol as a matrix. C,H,N analyses were performed by H. Feuerhake (Universität des Saarlandes).

2-(2-Hydroxyphenyl)-benzo-4*H*-[1,3]-oxazin-4-one:[43] Salicylic acid (24.9 g, 0.18 mol), salicylamide (20.6 g, 0.15 mol) and pyridine (1.5 mL) were refluxed in xylene (30 mL). Thionyl chloride (23.7 mL, 0.33 mol) was added with vigorous stirring over a period of 4 h. An intense evolution of SO_2 and HCl was noted. At the end of the addition, the product started to crystallize. Stirring was continued for an additional 30 min, and the xylene was removed by distillation at reduced pressure. The resulting solid residue was suspended in EtOH (60 mL) and acetic acid (1.5 mL). The mixture was heated gently and then allowed to cool to 20 °C. The precipitate was filtered and recrystallized from 2-methoxyethanol (70 mL). Yield: yellow needles (19.78 g, 82.7 mmol, 55%). The product decomposed slowly when exposed to moisture, forming bis(salicyl)-imide. $C_{14}H_9NO_3$ (239.2): calcd. C 70.29, H 3.79, N 5.85; found C 70.80, H 3.88, N 5.70. ^1H NMR ([D$_6$]DMSO): δ = 7.09 (m, 2 H), 7.62 (m; 2 H), 7.78 (d, 1 H), 7.94 (t, 1 H), 8.07 (d, 1 H), 8.20 (d, 1 H), 8.78 (OH) ppm. ^{13}C NMR ([D$_6$]DMSO): δ = 111.4, 117.4, 117.8, 117.9, 119.5, 126.7, 127.2, 129.0, 136.0, 136.7, 153.8, 161.8, 163.4, 164.8 ppm. UV/Vis (H_2O, 25 °C): λ_{max} = 371, 323 nm.

4-[3,5-Bis(2-hydroxyphenyl)-1,2,4-triazol-1-yl]benzoic Acid (H_3L^x):[19] 4-Hydrazino-benzoic acid (1.75 g, 11.5 mmol) and NEt_3 (1.16 g, 11.5 mmol) were dissolved in boiling EtOH (80 mL). To the clear solution was added 2-(2-Hydroxyphenyl)-4*H*-3,1-benzoxazin-4-one (2.50 g, 10.45 mmol), and the reaction mixture was refluxed for an additional 2 h. The solution was then allowed to cool to room temperature, and H_2O was added until some perturbation (i.e. a first sign of precipitation) was observed. The mixture was concentrated to a total volume of 50% under reduced pressure and aqueous 6 M HCl (40 mL) was added. The resulting solid was filtered and dried for 24 h in vacuo (3.11 g, 8.34 mmol, 80%). $C_{21}H_{15}N_3O_4$ (373.37): calcd. C 67.56, H 4.05, N 11.25; found C 67.76, H 3.85, N 11.14. ^1H NMR ([D$_6$]DMSO): δ = 6.90 (d, 1 H), 7.00−7.04 (m, 3 H), 7.37 (m, 2 H), 7.55 (d, 1 H), 7.58 (d, 2 H), 8.02 (d, 2 H), 8.08 (d, 1 H) 10.05 (s, OH), 10.81 (s, OH), 13.20 (broad, OH) ppm. ^{13}C NMR ([D$_6$]DMSO): δ = 113.6, 114.4, 116.2 (CH), 117.0 (CH), 119.4 (CH), 119.6 (CH), 123.2 (2 CH), 126.7 (CH), 130.2 (2 CH), 130.5, 131.0 (CH), 131.4 (CH), 132.5, 141.2 (CH), 152.0, 155.2, 156.4, 159.9, 166.4 ppm. UV/Vis (H_2O/DMSO, x_{DMSO} = 0.2, pH <2, 25 °C): λ_{max} (ε) = 284 nm (1.5×10^4), 296 (sh). FAB^+-MS: *m*/*z* = 374 (100%, $[H_4L^x]^+$). Single crystals of H_3L^x were grown by slow evaporation of a MeOH solution at room temperature. The solid was allowed to stand exposed to the air to form the monohydrate $H_3L^x{\cdot}H_2O$. $C_{21}H_{17}N_3O_5$ (391.39): calcd. C 64.45 H 4.38, N 10.74; found C 64.11, H 4.60, N 10.44.

4-[3,5-Bis(2-hydroxyphenyl)-1,2,4-triazol-1-yl]benzosulfonic Acid (H_3L^y):[20] 4-Hydrazino-benzosulfonic acid (2.4 g, 12.75 mmol) was suspended in EtOH (300 mL). The solid was dissolved by the addition of one equivalent of NEt_3 (1.29 g, 12.75 mmol). The solution was refluxed, and 2-(2-hydroxyphenyl)-4*H*-3,1-benzoxazin-4-one (3.00 g, 12.5 mmol) was added. Heating was continued for an additional 20 h. The clear solution was then allowed to cool to room temperature, and 6 M aqueous HCl (60 mL) was added. The resulting acidic solution was evaporated under reduced pressure until a white solid started to precipitate. A further portion of 6 M aqueous HCl (60 mL) was added. The solid was then separated by filtration and washed with a small portion of cold H_2O, and dried in vacuo over P_4O_{10} for 24 h (4.37 g, 10.67 mmol, 85%). $C_{20}H_{15}N_3O_5S$ (409.42): calcd. C 58.67, H 3.69, N 10.26; found C 58.99, H 3.90, N 9.88. ^1H NMR ([D$_6$]DMSO): δ = 6.91 (d, 1 H), 6.95−7.01 (m, 2 H), 7.05 (d, 1 H), 7.36−7.40 (m, 2 H), 7.46 (d, 2 H), 7.51 (d, 1 H), 7.72 (d, 2 H), 8.02 (d, 1 H) ppm. ^{13}C NMR (DEPT90, [D$_6$]DMSO): δ = 113.3, 113.4, 116.4 (CH), 117.1 (CH), 119.5 (CH), 119.8 (CH), 123.4 (2 CH), 126.7 (2 CH), 127.4 (CH), 131.2 (CH), 131.9 (CH), 132.9 (CH), 137.7, 148.1, 151.6, 155.5, 156.4, 158.4 ppm. UV/Vis (H_2O; pH <2; 25 °C): λ_{max} (ε) = 255 (1.4×10^4); 295 nm (1.2×10^4). FAB^+-MS: *m*/*z* = 410 (100) $[H_4L^y]^+$. The solid was allowed to stand exposed to the air, which resulted in the formation of the monohydrate $H_3L^y{\cdot}H_2O$. $C_{20}H_{17}N_3O_6S$ (427.44): calcd. C 56.20, H 4.01, N 9.83; found C 56.02, H 4.24, N 9.61.

3,5-Bis(2-hydroxyphenyl)-1-phenyl-1,2,4-triazole (H_2L^z):[43] Phenylhydrazine hydrochloride (1.45 g, 10.03 mmol) was dissolved in boiling EtOH (80 mL). 2-(2-hydroxyphenyl)-4*H*-3,1-benzoxazin-4-one (2.0 g, 8.36 mmol) was added, and the resulting clear yellow solution was heated under reflux for an additional 2 h. The yellow color disappeared, and the colorless solution was allowed to cool to room temperature. Addition of aqueous 1 M HCl (40 mL) resulted in precipitation of a white solid, which was filtered off and dried for 12 h in vacuo. Recrystallization from hot MeOH yielded a crystalline material that was suitable for single-crystal X-ray analysis. Yield: (1.72 g, 5.23 mmol, 62.5%). $C_{20}H_{15}N_3O_2$ (329.36): calcd. C 72.94, H 4.59, N 12.76; found C 72.61, H 4.36, N 12.64.

^{1}H NMR ([D$_6$]DMSO): δ = 6.89 (d, 1 H), 6.94 (t, 1 H), 6.98−7.04 (m, 2 H), 7.37 (t, 2 H), 7.42−7.48 (m, 6 H), 7.85 (d, 1 H), 9.88 (s, OH), 10.71 (s, OH) ppm. ^{13}C NMR ([D$_6$]DMSO): δ = 113.7, 114.5, 116.0, 116.9, 119.1, 119.4, 123.6 (2 CH), 126.5, 128.5, 129.0 (2 CH), 130.8, 131.1, 132.1, 137.7, 151.6, 155.3, 156.2, 159.4 ppm. UV/Vis (H$_2$O/DMSO, x_{DMSO} = 0.2; pH <7; 25 °C): λ_{max} (ε) = 255 (1.5 × 10^4); 300 nm (1.2 × 10^4). MS-EI$^+$: m/z = 329.4 (100) [H$_2$L^z]$^+$.

Na[Fe(L^z)$_2$]·2H$_2$O·C$_2$H$_5$OH: FeCl$_3$ (324 mg, 2 mmol) dissolved in abs. EtOH (15 mL) was added to a solution of H$_2$L^z (660 mg, 2 mmol) in ethanol (15 mL). The resulting solution turned deep purple, indicating the formation of the 1:1 complex [Fe(L^z)]$^+$. In a separate reaction, solid Na was added to abs. EtOH to saturation.This NaOEt solution (1 mL) was then layered with the Fe^{III}−L^x solution (0.5 mL). After some hours, the deposition of deep red crystals was observed at the boundary of the two phases. It is important that the crystals remained in this intermediate medium and do not sink into the NaOEt solution. They were subsequently removed and immediately cooled to 100 K for the X-ray diffraction study. The single crystal analysis established the composition as Na[Fe(L^z)$_2$]·4C$_2$H$_5$OH. However, the crystal disintegrated rapidly and the compound that formed had the composition Na[Fe(L^z)]·2H$_2$O·C$_2$H$_5$OH. C$_{42}$H$_{36}$FeN$_6$NaO$_7$ (815.63): calcd. C 61.85, H 4.45, N 10.30; found C 62.49, H 4.15, N 10.02. FAB$^+$-MS: m/z = 709.5−714.5 (20%, superposition of [Fe(L^z)$_2$]$^+$, [Fe(L^z)(HL^z)]$^+$, [Fe(HL^z)$_2$]$^+$), 731.5−736.5 (100%, superposition of [NaFe(L^z)$_2$]$^+$ and [NaFe(L^z)(HL^z)]$^+$), 754.5−758.5 (79%, [Fe(L^z)$_2$(EtOH)]$^+$).

Na[Al(L^z)$_2$]·H$_2$O·C$_2$H$_5$OH: The procedure reported for the preparation of the corresponding Fe^{III} complex was used. Single crystals of composition Na[Al(L^z)$_2$]·4C$_2$H$_5$OH were obtained. They disintegrated rapidly to form Na[Al(L^z)$_2$]·H$_2$O·C$_2$H$_5$OH. C$_{42}$H$_{34}$AlN$_6$NaO$_6$ (768.75): calcd. C 65.62, H 4.46, N 10.93; found C 65.73, H 4.20, N 10.56.

Cu(L^z):[21] CuBr$_2$ (223 mg, 1 mmol) was added to a solution of H$_2$L^z (329 mg, 1 mmol) in EtOH (10 mL). The mixture was stirred until a green solid precipitated. The precipitation was completed by adding a concentrated solution of NaOMe in MeOH. Yield 290 mg (742 μmol, 74%). C$_{20}$H$_{13}$CuN$_3$O$_2$ (390.89): calcd. C 61.46, H 3.35, N 10.75; found C 61.96, H 3.35, N 10.73.

[Cu(L^z)(pyridine)]$_2$: The procedure, reported by Uhlemann and coworkers[44] for the preparation of a Cu^{II} complex with a related tridentate [O,N,O]-ligand, was used with some minor modifications: Solid Cu(L^z) (290 mg, 742 μmol) was dissolved in boiling pyridine (20 mL). This solution (2 mL) was mixed with MeOH (1 mL). H$_2$O (100 μL) was then layered on the resulting green solution. Dark green crystals of [Cu(L^z)(pyridine)]$_2$ suitable for single-crystal X-ray analysis grew within 24 h at 4 °C.

Potentiometric Measurements: All titrations were carried out at an ionic strength of 0.1 M (KCl or KNO$_3$) using a Metrohm 665 piston burette, a Metrohm 6.0222.100 glass electrode with an incorporated Ag/AgCl reference (aqueous), and a Metrohm 713 pH/mV meter. The pH meter and the piston burette were controlled by a PC.[45] The samples (50 mL) were placed in a double-jacketed beaker, and the temperature was maintained at 25.0 ± 0.1 °C using a Lauda ecoline103 thermostat. KOH (0.10 M, Merck Titrisol) having the same H$_2$O/DMSO molar ratio as the corresponding sample solution was used as titrant. The H$_2$O/DMSO samples were prepared using published values of the partial molar volumes of the two components (the H$_2$O/DMSO mixtures show a significant deviation from ideal behavior).[46] Titrations of the Fe^{II} complexes were performed under Ar, which was scrubbed with an alkaline solution of pyrogallol to remove traces of O$_2$. The other titrations were performed under N$_2$, which was passed through a 0.1 M aqueous KCl solution. The apparent ionization constant of the different H$_2$O/DMSO media was determined by multiple acid−base titrations. The pK_as of the ligands were measured using solid, analytically pure samples of H$_3$L^x, H$_3$L^y, and H$_2$L^z. The formation constants of the ferric complexes were determined using stock solutions of the ligands (0.01 M), which were standardized by acid−base titrations, and stock solutions of Fe^{III}, which were standardized photometrically as tris-phenanthroline-Fe^{II}.[47] Additional acid (HCl or HNO$_3$) was added to the Fe^{III} stock solutions to prevent partial hydrolysis prior to the titration. Complex formation with Fe^{III} was found to be sluggish, and additional back titrations were performed to ensure complete equilibration. A measuring time of 800−920 s per point proved necessary to avoid a significant hysteresis. Total ligand and total Fe concentrations ranged from 5×10^{-4} to 2×10^{-3} M.[48]

Spectrophotometric Titrations: The titration cell used for potentiometry was equipped with an immersion probe (HELLMA), which was connected to a diode array spectrophotometer (J&M, TIDAS-UV/NIR/100−1). A PC was used to trigger the recording of a spectrum just prior to the addition of each new aliquot of titrant.[45] For the pK_a determination of H$_3$L^x, H$_3$L^y, and H$_2$L^z, the total ligand concentration was about 10^{-5}−10^{-4} M, and absorption data in the range 250 < λ < 400 nm were collected. For the formation constants of the Fe^{III} complexes, total [Fe] was in the range 9.1×10^{-5}−3.5×10^{-4} M, and total [L] in the range 9.1×10^{-5}−9.7×10^{-4} M. The p$K_{a,1}$ of H$_3$L^y and the formation constants of [Fe(HL^x)]$^+$, [Fe(L^y)], and [Fe(L^z)]$^+$ were determined by a batch method with 10−40 individually sealed 10-mL samples in the range 1 < pH < 2 (25.0 °C) allowing an equilibration time of 24 h.[48]

Calculations of Equilibrium Constants: The computer programs HYPERQUAD[49] and SPECFIT[50] were used to evaluate the potentiometric and spectrophotometric data, respectively. All equilibrium constants were calculated as concentration constants, and pH was defined as −log [H$^+$]. For pure aqueous solutions, a pK_w of 13.78 was used.[36] In H$_2$O/DMSO solutions, the apparent ionization constant Q_c = [H$^+$]×[OH$^-$] depended linearly on x_{DMSO} in the range 0.1 ≤ x_{DMSO} ≤ 0.2 with pQ_c = 14.65 (x_{DMSO} = 0.10) and pQ_c = 15.59 (x_{DMSO} = 0.20). These values are in good agreement with those reported in the literature.[27] A graphical representation of pQ_c versus x_{DMSO} is shown in the supporting information (Figure S2). The pK_w (or pQ_c) and the total concentrations of the reactants were always treated as fixed values. Additionally, the protonation constants of the ligands were fixed when refining formation constants of metal-containing species. Because Fe(NH$_4$)$_2$(SO$_4$)$_2$·6H$_2$O was used as a Fe^{II} source, the pK_a of NH$_4^+$ was determined to be 8.90 (x_{DMSO} = 0.2). However, the formation of [Fe^{II}(L^y)]$^-$, which was investigated in the range of 5.9 < pH < 6.9, did not interfere with the deprotonation of NH$_4^+$. For the evaluation of the spectrophotometric titrations, the spectrum of free Fe^{3+} was measured separately for each H$_2$O/DMSO ratio, and was then imported and treated as fixed during refinement. Only absorption data with λ >400 nm were used for the evaluation of metal complex formation, and the free ligands and their protonation products could therefore be considered as colorless (see Figures S3 and S4).

Electrochemistry: Cyclic voltammograms were recorded in H$_2$O or H$_2$O/DMSO (x_{DMSO} = 0.2) using 0.1 M KCl as supporting electrolyte at ambient temperature (23 ± 3 °C). A BAS C2 cell equipped with a BAS 100B/W 2 potentiostat, a Pt counter electrode, and an

Table 4. Crystallographic data for ICL670 (H_3L^x), $Na[Fe(L^z)_2]\cdot 4EtOH$, and $[Cu(L^z)(pyridine)]_2$

	ICL670	$Na[Fe(L^z)_2]\cdot 4EtOH$	$[Cu(L^z)(pyridine)]_2$
Empirical formula	$C_{21}H_{15}N_3O_4$	$C_{48}H_{50}FeN_6NaO_8$	$C_{50}H_{36}Cu_2N_8O_4$
Molecular weight	373.36	917.78	939.95
Crystal system	monoclinic	monoclinic	monoclinic
Space group	$P2_1/c$ (No. 14)	$C2/c$ (No. 15)	$P2_1/c$ (No. 14)
a [Å]	8.900(2)	23.933(4)	10.944(2)
b [Å]	26.946(5)	8.7399(12)	10.476(2)
c [Å]	7.558(2)	24.166(4)	18.419(4)
β [°]	94.77(3)	107.84(3)	100.05(3)
V [Å^3]	1806.3(7	4811.8(13)	2079.3(7)
Z	4	4	2
T [K]	215(2)	100(2)	293(2)
$D_{calcd.}$ [g cm^{-3}]	1.373	1.267	1.501
μ [mm^{-1}]	0.097	0.380	1.082
Crystal size [mm]	0.3 × 0.2 × 0.2	0.35 × 0.18 × 0.18	0.08 × 0.05 × 0.02
θ_{min}, θ_{max}	2.42, 24.13	1.79, 24.00	2.25, 23.99
Trans (min., max)	−	0.5567, 0.9625	−
Data set	−10/10; −30/30; −8/8	−28/24; −10/9; −27/26	−11/11; −11/11; −20/21
Total/Unique data	11218, 2810	9450, 3738	12786, 3077
Parameter/Restraints	313/0	269/9	289/0
R_1, wR_2, [$I > 2\sigma(I)$]	0.0468, 0.1033	0.0870, 0.2352	0.0599, 0.1143
R_1, wR_2, (all data)	0.0755, 0.1133	0.1456, 0.2832	0.1595, 0.1450
Max. peak/hole [e/ Å^3]	0.227/−0.218	1.240/−0.550	0.375/−0.442

Ag/AgCl reference electrode was used. The total iron concentration was 2.5 mM. Measurements at pH <4 ($E > -200$ mV vs. Ag/AgCl) were performed using a Pt working electrode. For the high pH samples (pH >6, $E < -400$ mV vs. Ag/AgCl) a hanging Hg drop working electrode was used.

Crystal Structure Determination:[51] X-ray diffraction data of H_3L^x (215 K), $Na[Fe(L^z)_2]\cdot 4EtOH$ (293 K),[23] and $[Cu(L^z)(pyridine)]_2$ (293 K) were collected on a STOE IPDS diffractometer. Data collection of $Na[Al(L^z)_2]\cdot 4EtOH$ was performed on a Siemens SMART CCD diffractometer at 293(2) K. Additionally, a data set of the Fe complex was collected at 100(2) K on the SMART CCD diffractometer. Graphite monochromated Mo-K_α radiation (λ = 0.71073 Å) was used for all structures. Crystallographic data for H_3L^x, the Fe complex at 100 K, and the Cu complex are summarized in Table 4. The Al complex proved to be isotypic with the Fe complex; however, the reflections were rather weak, and the data could not be refined satisfactorily.[24] All data sets were corrected for Lorentz and polarization effects, and an absorption correction was applied to the data of the Fe complex collected at 100 K. Minimal and maximal transmission factors were 0.5567 and 0.9625. All structures were solved by direct methods (SHELXS-97) and refined by full-matrix least-squares calculations on F^2 (SHELXL-97).[52] Anisotropic displacement parameters were refined for all non-hydrogen atoms of H_3L^x and $[Cu(L^z)(pyridine)]_2$. In the low-temperature structure of the Fe complex, the $[Fe(L^z)_2]^-$ anion was modeled as a superposition of two orientations, having the Fe center, the phenoxo rings, and the C−N−C moieties of the triazole rings in common. For the two outer nitrogen atoms (N2 and N3) and the peripheral phenyl ring, a major (66%) and a minor (34%) component were located. Non-hydrogen atoms of the nondisordered part and of the major component (except N2 and N3) of the anion, as well as the Na position and the C and O positions of a nondisordered EtOH molecule were refined with anisotropic displacement parameters. All C and N atoms of the minor component, N2 and N3 of the major component, and the C and O position of a second, disordered EtOH molecule were refined isotropically. The hydroxy hydrogen atom H(80) of the nondisordered EtOH was located and refined isotropically with $U_{iso} = 1.3 \times U_{eq}$ of the oxygen atom. All other H atom positions of the two metal complexes were calculated (riding model). Isotropic displacement parameters were used with $U_{iso} = 1.5 \times U_{eq}$(C) for methyl groups and $U_{iso} = 1.2 \times U_{eq}$(C) for all other hydrogen atoms. The H atom positions of H_3L^x could all be located. They were successfully refined with variable isotropic displacement parameters.

Acknowledgments

X-ray diffraction data for H_3L^x (ICL670), $Na[Fe(L^z)_2]\cdot 4EtOH$ (293 K) and $[Cu(L^z)(pyridine)]_2$ were recorded by Dr. Volker Huch (Saarbrücken). The structure of $[Cu(L^z)(pyridine)]_2$ was solved and refined by Dr. Jürgen Sander (Saarbrücken). Some of the CV measurements were performed by Michael Krämer (Saarbrücken). We thank Prof. G. Schwitzgebel (Saarbrücken, retired) for helpful discussions in interpreting the CV measurements, and Dr. Peter Osvath (Melbourne) for valuable advice.

[1] R. Crichton, *Inorganic Biochemistry of Iron Metabolism − From Molecular Mechanisms to Clinical Consequences*, 2nd Edition, John Wiley, Chichester, **2001**.
[2] [2a] Z. D. Liu, R. C. Hider, *Coord. Chem. Rev.* **2002**, *232*, 151. [2b] Z. D. Liu, R. C. Hider, *Med. Res. Rev.* **2002**, *22*, 26.
[3] R. C. Hider, Z. D. Liu, *Curr. Med. Chem.* **2003**, *10*, 1051.
[4] E. Nisbet-Brown, N. F. Olivieri, P. J. Giardina, R. W. Grady, E. J. Neufeld, R. Sechaud, A. J. Krebs-Brown, J. R. Anderson, D. Alberti, K. C. Sizer, D. G. Nathan, *Lancet* **2003**, *361*, 1597.
[5] [5a] C. Hershko, A. M. Konijn, H. P. Nick, W. Breuer, Z. I. Cabantchik, G. Link, *Blood* **2001**, *97*, 1115. [5b] H. Nick, P. Acklin, R. Lattmann, P. Buehlmayer, S. Hauffe, J. Schupp, D. Alberti, *Curr. Med. Chem.* **2003**, *10*, 1065.
[6] R. S. Britton, K. L. Leicester, B. R. Bacon, *Int. J. Hematol.* **2002**, *76*, 219.
[7] S. I. Liochev, *Met. Ions Biol. Syst.* **1999**, *36*, 1.
[8] M. J. Burkitt, *Prog. React. Kinet. Mech.* **2003**, *28*, 75.
[9] H. B. Dunford, *Coord. Chem. Rev.* **2002**, *233−234*, 311.
[10] [10a] W. H. Koppenol, *Redox Rep.* **2001**, *6*, 229. [10b] S. I. Liochev, I. Fridovich, *Redox Rep.* **2002**, *7*, 55.

[11] W. H. Koppenol, *Redox Rep.* **2001**, *6*, 339.
[12] S. Y. Qian, G. R. Buettner, *Free Radic. Biol. Med.* **1999**, *26*, 1447.
[13] S. J. Stohs, D. Bagchi, *Free Radic. Biol. Med.* **1995**, *18*, 321.
[14] [14a] S. Toyokuni, *Free Radic. Biol. Med.* **1996**, *20*, 553. [14b] R. Meneghini, *Free Radic. Biol. Med.* **1997**, *23*, 783.
[15] B. P. Esposito, W. Breuer, P. Sirankapracha, P. Pootrakul, C. Hershko, Z. I. Cabantchik, *Blood* **2003**, *102*, 2670.
[16] M. Fontecave, J. L. Pierre, *Bull. Soc. Chim. Fr.* **1993**, *130*, 77.
[17] U. Heinz, K. Hegetschweiler, P. Acklin, B. Faller, R. Lattmann, H. P. Schnebli, *Angew. Chem.* **1999**, *111*, 2733; *Angew. Chem. Int. Ed.* **1999**, *38*, 2568.
[18] [18a] A.-F. Miller, *Compr. Coord. Chem. II* **2004**, *8*, 479. [18b] D. R. Lide (Ed.), *CRC Handbook of Chemistry and Physics 83rd Edition 2002−2003*, CRC-Press, Washington D. C. **2002**.
[19] R. Lattmann, P. Acklin (Novartis Pharma AG), PCT Int. Appl. WO 9749395 A1 **1997** [*Chem. Abstr.* **1998**, *128*, 114953e].
[20] F. Bachmann, J. Dannacher, G. Schlingloff, M. Hazenkamp, G. Haensler, K. Hegetschweiler, U. Heinz, (Ciba Specialty AG), PCT Int. Appl. WO 2003053986 A1 **2003** [*Chem. Abstr.* **2003** 139, 87009].
[21] Y. I. Ryabukhin, N. V. Shibaeva, A. S. Kuzharov, V. G. Korobkova, A. V. Khokhlov, A. D. Garnovskii, *Koord. Khim.* **1987**, *13*, 869; English Translation: *Soviet J. Coord. Chem.* **1987**, *13*, 493.
[22] U. Heinz, J. Sander, K. Hegetschweiler, *Z. Kristallogr. New Cryst. Struct.* **2001**, *216*, 113.
[23] Crystal data: $C_{48}H_{50}FeN_6NaO_8$, a = 24.138(5), b = 8.855(2), c = 24.597(5), β = 107.77(3), V = 5006.6(18), Z = 4, T = 293(2) K, space group $C2/c$, reflections: 15286 collected, 3741 unique, 2689 observed with $I > 2\sigma(I)$. R_1(observed data) = 0.1224, wR_2(all data) = 0.3476.
[24] Crystal data: $C_{48}H_{50}AlN_6NaO_8$, a = 23.922(9), b = 8.712(3), c = 24.168(10), β = 107.26(3), V = 4810.0(32), Z = 4, T = 293(2) K, space group $C2/c$, reflections: 7299 collected, 2578 unique, 1232 observed with $I > 2\sigma(I)$. R_1(observed data) = 0.1402, wR_2(all data) = 0.4545.
[25] [25a] Z. Travnicek, Z. Sindelar, J. Marek, *Z. Kristallogr. New Cryst. Struct.* **1997**, *212*, 125. [25b] I. Vencato, A. Neves, B. R. Vincent, C. Erasmus-Buhr, W. Haase, *Acta Crystallogr., Sect. C* **1994**, *50*, 386. [25c] B. S. Snyder, G. S. Patterson, A. J. Abrahamson, R. H. Holm, *J. Am. Chem. Soc.* **1989**, *111*, 5214. [25d] T. Weyhermüller, T. K. Paine, E. Bothe, E. Bill, P. Chaudhuri, *Inorg. Chim. Acta* **2002**, *337*, 344. [25e] H. Aneetha, K. Panneerselvam, T.-F. Liao, T.-H. Lu, C.-S. Chung, *J. Chem. Soc., Dalton Trans.* **1999**, 2689.
[26] [26a] M. T. Garland, J. Y. Le Marouille, E. Spodine, *Acta Crystallogr., Sect. C* **1985**, *41*, 855. [26b] P. Lemoine, D. Nguyen-Huy, B. Viossat, J.-M. Leger, A. Tomas, *Acta Crystallogr., Sect. C* **1999**, *55*, 2068. [26c] R. M. Buchanan, C. Wilson-Blumenberg, C. Trapp, S. K. Larsen, D. L. Greene, C. G. Pierpont, *Inorg. Chem.* **1986**, *25*, 3070. [26d] N. Matsumoto, M. Mimura, Y. Sunatsuki, S. Eguchi, Y. Mizuguchi, H. Miyasaka, T. Nakashima, *Bull. Chem. Soc., Jpn.* **1997**, *70*, 2461. [26e] Y. Sunatsuki, M. Nakamura, N. Matsumoto, F. Kai, *Bull. Chem. Soc., Jpn.* **1997**, *70*, 1851. [26f] C. A. Otter, S. M. Couchman, J. C. Jeffery, K. L. V. Mann, E. Psillakis, M. D. Ward, *Inorg. Chim. Acta* **1998**, *278*, 178. [26g] Y. Sunatsuki, T. Matsuo, M. Nakamura, F. Kai, N. Matsumoto, J.-P. Tuchagues, *Bull. Chem. Soc., Jpn.* **1998**, *71*, 2611. [26h] A. Bavoso, L. Menabue, M. Saladini, M. Sola, *Inorg. Chim. Acta* **1996**, *244*, 207. [26i] P. Lemoine, A. Mazurier, I. Billy, D. Nguyen-Huy, B. Viossat, *Z. Kristallogr. New Cryst. Struct.* **2000**, *215*, 523.
[27] [27a] E. M. Woolley, L. G. Hepler, *Anal. Chem.* **1972**, *44*, 1520. [27b] P. Fiordiponti, F. Rallo, F. Rodante, *Z. Phys. Chem.* **1974**, *88*, 149.
[28] T. Eicher, S. Hauptmann, *The Chemistry of Heterocycles*, 2nd edn, WILEY-VCH, Weinheim, **2003**.
[29] A. E. Martell, R. D. Hancock, *Determination and Use of Stability Constants*, 2nd Edition, VCH Publishers, New York, **1992**.
[30] W. R. Harris, K. N. Raymond, F. L. Weitl, *J. Am. Chem. Soc.* **1981**, *103*, 2667.
[31] [31a] J. N. Butler, *J. Electroanal. Chem.* **1967**, *14*, 89. [31b] D. T. Sawyer, J. L. Roberts, Jr., *Experimental Electrochemistry for Chemists*, John Wiley, **1974**, New York.
[32] [32a] K. Hegetschweiler, M. Ghisletta, L. Hausherr-Primo, T. Kradolfer, H. W. Schmalle, V. Gramlich, *Inorg. Chem.* **1995**, *34*, 1950. [32b] K. Hegetschweiler, M. Weber, V. Huch, M. Veith, H. W. Schmalle, A. Linden, R. J. Geue, P. Osvath, A. M. Sargeson, A. C. Willis, W. Angst, *Inorg. Chem.* **1997**, *36*, 4121.
[33] A. E. Martell, R. D. Hancock, *Metal Complexes in Aqueous Solutions*, Plenum Press, New York, **1996**.
[34] R. G. Pearson, *Chemical Hardness*, WILEY-VCH, New York, **1997**.
[35] [35a] R. D. Hancock, *Prog. Inorg. Chem.* **1989**, *37*, 187. [35b] R. D. Hancock, *Acc. Chem. Res.* **1990**, *23*, 253.
[36] R. M. Smith, A. E. Martell, R. J. Motekaitis, *Critically Selected Stability Constants of Metal Complexes*, NIST Standard Reference Database 46; Version 7.0; Gaithersburg, MD, USA **2003**.
[37] P. Paoletti, R. Walser, A. Vacca, G. Schwarzenbach, *Helv. Chim. Acta* **1971**, *54*, 243.
[38] K. Hegetschweiler, *Chem. Soc. Rev.* **1999**, *28*, 239.
[39] The minor differences between the two ligands L^x and L^y can be ignored for these rather general considerations.
[40] R. D. Shannon, *Acta Crystallogr., Sect. A* **1976**, *32*, 751.
[41] It can be assumed that a hypothetical protonated complex $[Fe^{II}(L^x)(HL^x)]^{3-}$ would in any case be more acidic than the free ligand HL^{2-}.
[42] A. El-Jammal, D. M. Templeton, *Inorg. Chim. Acta* **1996**, *245*, 199.
[43] Yu. I. Ryabukhin, L. N. Faleeva, V. G. Korobkova, *Chem. Heter. Com.* (Engl. Trans.) **1983**, *19*, 332.
[44] E. Ludwig, U. Schilde, E. Uhlemann, H. Hartl, I. Brüdgam, *Z. Anorg. Allg. Chem.* **1996**, *622*, 701.
[45] *Messlabor, a computer program for the control of potentiometric and spectrophotometric titrations*, Scientec GmbH, Saarbrücken, **2002**.
[46] J. T. W. Lai, F. W. Lau, D. Robb, P. Westh, G. Nielsen, C. Trandum, A. Hvidt, Y. Koga, *J. Solution Chem.* **1995**, *24*, 89.
[47] A. I. Vogel, *A Textbook of Quantitative Inorganic Analysis*, 5th edn, Longmans, London, **1987**.
[48] Further details of the titration experiments (Tables S1−S13 and Figures S3, S4, S6−S8) are provided as Supporting Information.
[49] P. Gans, A. Sabatini, A. Vacca, *Talanta* **1996**, *43*, 1739.
[50] [50a] R. A. Binstead, B. Jung, A. D. Zuberbühler, SPECFIT/32 Version 3.0, Spectrum Software Associates, Marlborough, MA 01752, USA, **2000**. [50b] H. Gampp, M. Maeder, C. J. Meyer, A. D. Zuberbühler, *Talanta* **1985**, *32*, 95.
[51] Crystallographic data (excluding structure factors) for $Na[Fe(L^z)_2]\cdot 4EtOH$ (293 K), $[Cu(L^z)(pyridine)]_2$, H_3L^x (ICL670), $Na[Fe(L^z)_2]\cdot 4EtOH$ (100 K), and $Na[Al(L^z)_2]\cdot 4EtOH$ (293 K) have been deposited with the Cambridge Crystallographic Data Center as supplementary publication nos. CCDC 237449−237453. Copies of the data can be obtained free of charge on application to CCDC, 12 Union Road, Cambridge CB2 1EZ, UK [Fax (internat.): +44-1223-336033; E-mail: deposit@ccdc.cam.ac.uk].
[52] [52a] G. M. Sheldrick, *SHELXS-97 Program for Crystal Structure Solution*, Göttingen, **1990**. [52b] G. M. Sheldrick, *SHELXL-97 Program for Crystal Structure Refinement*, Göttingen, **1997**.

Received May 4, 2004
Early View Article
Published Online September 13, 2004

